Fuel 414 (2026) 138434

Contents lists available at ScienceDirect

Fuel

journal homepage: www.elsevier.com/locate/fuel

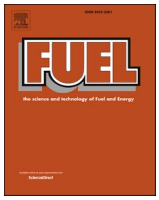

Full Length Article

Machine learning-based prediction and optimization of performance and emission characteristics in CI engines fueled by pumpkin seed biodiesel with thermal barrier coating and cerium oxide nanoparticles

V.S. Shaisundaram [a], Saravanakumar Sengottaiyan [b,*], R. Aruna [c], R. Muraliraja [a,*]

[a] Research Faculty, Department of Mechanical Engineering, Vels Institute of Science Technology and Advanced Studies, Chennai, India
[b] Faculty of Engineering and Technology, Villa College, Male 20002, Maldives
[c] Department of Information Technology, Kongunadu College of Engineering and Technology, Trichy, India

ARTICLE INFO

Keywords:
Thermal Barrier Coating
Pumpkin Seed Biodiesel
Cerium Oxide Nanoparticles
CI Engine Performance
Artificial Neural Network
Response Surface Methodology

ABSTRACT

This study investigates the combined influence of a yttria-stabilized zirconia (YSZ)-based thermal barrier coating (TBC) and cerium oxide (CeO_2) nanoparticles on the performance and emissions of a compression ignition (CI) engine operated using pumpkin seed biodiesel blends. A multidisciplinary approach integrating experimental evaluation, machine learning prediction, and statistical optimization is employed. The coating system comprises a YSZ–Al_2O_3–CeO_2 composite layer applied via plasma spraying, while CeO_2 nanoparticles (35–55 ppm) are dispersed in PSB–diesel blends using surfactant-assisted ultrasonication. Engine tests were conducted across biodiesel blends (B10–B30) and four load levels (50–100%). A feed-forward ANN with three input neurons, two hidden layers (optimized through grid search), and one output neuron was trained to predict SFC, BTE, CO, HC, NOx, and smoke with high accuracy ($R^2 > 0.99$). A user-defined RSM (L27) design was used for multi-response optimization, constrained to maximize BTE while minimizing SFC and emissions. The optimal conditions, B30, 52% load, and 50 ppm CeO_2, resulted in reduced SFC (0.316 kg/kWh), enhanced BTE (24.87%), and substantial emission reductions. Novelty arises from the integration of non-edible pumpkin seed biodiesel, CeO_2-enhanced nanofuels, a composite TBC, and a hybrid ANN–RSM predictive–optimization framework, which collectively demonstrate a viable pathway toward cleaner and more efficient CI engine operation.

1. Introduction

The world's potential for sustainable green energy is increasing at an unprecedented rate due to the rapid growth of population, urbanization, and industrialization, along with a rise in global demand for sustainable and environmentally friendly energy sources [1–3]. Historically, conventional fossil fuels, particularly diesel, have been the workhorse of the transportation and power sectors, thanks to their high energy density and existing infrastructure [4–6]. Despite this, the large-scale use of these products leads to significant emissions of greenhouse gases (GHG), air pollution, and climate change [7–9]. This growing environmental concern, along with limited fossil fuel resources, has driven the search for alternative, renewable fuels that can meet energy demand while simultaneously reducing the environmental burden [10,11]. Vegetable oils, animal fats, and waste oils, as well as by-products from their processing, are used as renewable biological sources to produce biodiesel, an alternative to petroleum diesel [12–15]. Its biodegradability, low toxicity, and ability to decrease CO_2 emissions make it a desirable option for cleaner combustion [16–18]. However, in practical applications, the use of biodiesel faces challenges such as increased viscosity, lower calorific value, and engine adaptability, which may alter combustion characteristics and emissions from engines [19–21].

In response, recent research has focused on integrating advancements in nanotechnology and materials science with fuel formulations and engine design. Nano-additives, especially metal oxide nanoparticles like cerium oxide (CeO2), have demonstrated promising abilities to improve combustion by enhancing fuel atomization, promoting catalytic oxidation, and decreasing pollutant emissions [22–25]. CeO_2 possesses a high oxygen storage capacity and remarkable catalytic ability; utilizing such a material will effectively promote combustion, ultimately resulting in decreased emissions of unburned hydrocarbons (HC), carbon monoxide (CO), and particulates [26–29]. Similarly, thermal barrier

* Corresponding authors.
E-mail addresses: sskmechanical@gmail.com (S. Sengottaiyan), muralimechraja@gmail.com (R. Muraliraja).

https://doi.org/10.1016/j.fuel.2026.138434
Received 10 June 2025; Received in revised form 24 November 2025; Accepted 14 January 2026
Available online 17 January 2026

coatings (TBCs), which have been applied to engine components like pistons and cylinder liners, have garnered attention due to their potential to minimize heat loss during the combustion process [30–32]. TBCs help increase in-cylinder temperatures, which in turn enhance thermal efficiency and fuel utilization, leading to improved engine performance and reduced fuel consumption [33,34]. Generally made of ceramic materials, such as yttria-stabilized zirconia (YSZ), these coatings provide thermal insulation and protect metal components from thermal fatigue and corrosion [35]. Despite these advantages, challenges related to coating durability, thermal expansion mismatch, and long-term performance under cyclic engine conditions still need to be addressed [36]. The simultaneous application of nano-additives and thermal barrier coatings could serve as a synergistic strategy to overcome the limitations of using biodiesel in CI engines.

In this study, an attempt has been made to understand the effect of adding cerium oxide nanoparticles in dual-fuel mode with thermal barrier coatings on the performance and emission characteristics of a twin-cylinder direct-injection (DI) diesel engine fueled with 100% effective load of pumpkin seed biodiesel. Unlike previous investigations such as Anjaneya et al. [30], which focused solely on RSM-based optimization of biodiesel in coated engines, and Shaisundaram et al. [31], which examined Al_2O_3 nano-additives in diesel without machine-learning integration, the present study uniquely combines CeO_2 nano-additives, YSZ thermal barrier coatings, and pumpkin-seed biodiesel within an ANN–RSM hybrid modeling framework. This comprehensive integration provides both predictive and optimization insights, representing an advancement beyond prior TBC-based biodiesel studies. The goals are to increase brake thermal efficiency, reduce specific fuel consumption, and decrease energetically toxic emissions such as CO, HC, and nitrogen oxides (NOx), as well as smoke opacity.

This work contributes to the advancement of cleaner diesel engine systems and the development of sustainable industry and practices for the clean energy concept in a world where environmental pollution has become a crucial issue that must be addressed. Extensive research has been conducted to explore the synergistic effects of biodiesel blends combined with nano-additives and TBC on diesel engine performance and emissions. Numerous studies have demonstrated that incorporating ceramic-based TBCs, such as yttria-stabilized zirconia (YSZ) and alumina, along with metal oxide nanoparticles like CeO_2 and aluminum oxide (Al_2O_3), can significantly enhance combustion efficiency and reduce harmful exhaust emissions. Table 1 summarizes contemporary investigations in which various biodiesel feedstocks, ranging from palm, rapeseed, and jatropha to waste cooking oil and pumpkin seed oil, were tested under different coating and nanoparticle configurations.

In summary, it is evident that all the research indicated improvements in brake thermal efficiency (BTE), reductions in specific fuel consumption (SFC), and decreases in pollutant emissions, including CO, HC, NOx, and smoke. For instance, palm biodiesel mixed with CeO_2 nanoparticles and YSZ–Al_2O_3 coatings on the piston and liner showed a 4.82% increase in BTE and a 20.57% decrease in SFC. Additionally, the incorporation of Ce-ZnO nanoparticles was found to enhance the BTE value by a substantial 20.6% for soybean biodiesel and reduce the SFC value by over 21%. Collectively, these experimental findings demonstrate the potential of using nanoparticle additives co-doped with thermal barrier coatings (TBCs) to achieve enhanced fuel combustion, lower emissions, and improved engine efficiency. However, variations in feedstock types, coating materials, nanoparticle concentrations, and engine operating conditions necessitate further research to tailor these applications to specific fuels, particularly to lesser-studied options such as pumpkin seed biodiesel in the context of this research.

While numerous studies have reported the positive effects of biodiesel blends on engine performance and emissions when combined with nano-additives and thermal barrier coatings (TBCs), there remains a significant gap in the literature. Most existing research has focused on commonly available feedstocks, such as palm, rapeseed, and soybeans, with limited exploration of non-food, unconventional oils like pumpkin

Table 1
Summary of literature survey.

Reference Article	Engine	Biodiesel Blend	TBC Coating Material	Performance Outcomes
[37]	DI Diesel Engine	Palm Biodiesel B20	YSZ–Al_2O_3 plasma-sprayed piston & liner	Brake Thermal Efficiency (BTE) ↑4.82%, Specific Fuel Consumption (SFC) ↓20.57%, CO ↓15%, NOx ↓2.4%, HC ↓20%, Smoke ↓10%
[38]	Single-cylinder CI	*Cymbopogon flexuosus* biofuel B25 (25% blend)	Yttria-Stabilized Zirconia (YSZ)	BTE ↑1.75%, HC emissions ↓3.63%, CO↓4.75%, Smoke ↓5.05%, NOx slightly ↑ (amount not specified).
[39]	4-stroke, 1-cylinder DI CI engine	Mahua Biodiesel (MB100), Jatropha Biodiesel (JB100), Diesel	0.25 mm 7% YSZ top coat + 0.05 mm Ni-Cr-Al-Y bond coat (plasma spray)	BTE ↑2.7%, BSFC ↓3.1%, HC ↓6.9%, CO ↓6.5%, NOx ↑11.9% compared to baseline engine.
[40]	Kirloskar TV-1, single-cylinder CI	Diesel with Alumina nanoparticle additive (30 ppm)	Yttria Stabilized Zirconia (YSZ), plasma spray, 50 μm coating thickness	HC ↓10–15 ppm, CO ↓40%, NOx ↑2–5% (controlled with alumina nanoparticles), CO_2 ↑3–5%, optimal oxygen enrichment at 25%, improved combustion and engine performance with YSZ coating and alumina nanoparticle additives.
[41]	Kubota V3300, 4-cylinder, water-cooled CI engine	Green diesel blends: 10% Tucuma + 90% diesel, 10% Tungurahua + 90% diesel, 20% Tucuma + 80% diesel	Multilayered nano-structured thermal barrier coating: Alumina and YSZ, 200 μm thickness	Volumetric Efficiency ↑85%, BSFC ↓to 0.33 kg/kWh, CO ↓to 150 ppm, CO_2 ↓to 10.5%, NOx ↓to 300 ppm, BTE peaked around 36% at moderate loads, Emissions of hydrocarbons and smoke reduced compared to conventional fuels, Thermal barrier coatings with green diesel enhanced overall engine efficiency and combustion stability
[42]	Single-cylinder, 4-stroke DI diesel engine	Kariba weed biodiesel (90%) + n-pentane (10%) blend	Partially stabilized zirconia (plasma arc sprayed), 500 μm thickness	Brake thermal efficiency (BTE) increased by approximately 3% over the uncoated engine at high load; brake-specific

(*continued on next page*)

Table 1 (*continued*)

Reference Article	Engine	Biodiesel Blend	TBC Coating Material	Performance Outcomes
				fuel consumption (BSFC) decreased; CO, HC, and smoke emissions were significantly reduced; NOx emissions increased but were mitigated with the addition of n-pentane; the coated engine demonstrated improved combustion, higher in-cylinder pressure, and increased heat release rates; coating stability was confirmed after 100 h of operation.

seed oil for biodiesel production. Additionally, while the individual benefits of nano-additives and TBCs are well documented, there is a lack of detailed studies on their combined effect, particularly with CeO_2 nanoparticles in advanced composite TBCs, in engines fueled by pumpkin seed biodiesel. Furthermore, prior research typically addresses these factors in isolation, without integrating experimental validation, machine learning predictive modeling, and robust statistical optimization to comprehensively understand engine behavior under these complex conditions.

This study fills these gaps by exploring the performance of CeO_2 nanoparticles-enhanced pumpkin seed biodiesel in a thermal barrier-coated CI engine. The novelty of this work lies in the combination of an unconventional, non-food feedstock (pumpkin seed biodiesel) with nano-additives and TBCs, alongside the innovative hybridization of Artificial Neural Networks (ANN) and Response Surface Methodology (RSM) for optimization. The application of ANN allows for more accurate, real-time predictions of multiple engine parameters, while RSM provides a robust framework for multi-response optimization in the presence of non-linear variabilities. Additionally, this study uniquely investigates the long-term stability and performance of nano-additive-containing composite TBCs, offering new insights into their practical applications in biodiesel-powered engines. This data-driven approach marks a significant advancement in understanding and implementing sustainable, carbon–neutral biofuels and nanotechnology for cleaner, more efficient engine technologies.

2. Materials and methods

2.1. Preparation of pumpkin seed biodiesel (PSOME)

Pumpkin seed oil was selected because it is a non-edible, readily available agricultural by-product with a high lipid content (≈45–50%) suitable for biodiesel production. Its favorable fatty acid profile (rich in linoleic and oleic acids) supports efficient transesterification and yields biodiesel with good combustion characteristics. Prior studies have also indicated its promising engine performance and stability, making it an attractive and sustainable alternative feedstock for biofuel research [35,43]. The seeds, also known as pepitas, are used to produce oil containing beneficial components such as linoleic acid and vitamin E, making it a suitable feedstock for biodiesel production. Filtered pumpkin seed oil (PSO) is readily available in the domestic market, which has already undergone filtration to remove solid impurities. To ensure the oil is free from moisture and ready for the transesterification process, pumpkin seed oil was preheated to 60°C to remove any residual moisture [44]. The oil was then filtered to eliminate any suspended solids, ensuring its purity before undergoing transesterification.

The filtered oil was subjected to base-catalyzed transesterification using sodium methoxide, produced by reacting sodium hydroxide (NaOH) with methanol. The transesterification reaction was carried out at 65°C for 60 min with continuous stirring at 600 rpm to maintain homogeneity and facilitate the reaction. This process converts the triglycerides in the oil into methyl esters (biodiesel) and glycerol. After transesterification, the mixture was allowed to settle for 24 h in a separating funnel, enabling the biodiesel (PSOME) to separate from the glycerol. The top biodiesel layer was carefully collected, and the biodiesel was then subjected to several washes with warm distilled water at 65°C to remove any residual impurities such as excess methanol, soap, and glycerol. After washing, the biodiesel was dried at 105°C to eliminate any remaining moisture. Pumpkin seed biodiesel production is depicted in Fig. 1.

The properties of the obtained biodiesel (PSOME) were compared with ASTM standards and diesel. Table 2 shows the key physicochemical characteristics of pumpkin seed biodiesel (B100) and diesel. The comparison revealed that PSOME has a higher density (901.2 kg/m^3) and greater kinematic viscosity (5.8 cSt at 40°C) compared to diesel, which may influence its atomization and combustion characteristics.

The flash point (174°C) and fire point (190.2°C) of PSOME are significantly higher than those of diesel, making it safer for storage and handling. The gross calorific value of PSOME is slightly lower (40.3 MJ/kg) compared to diesel (43.4 MJ/kg), indicating a marginal reduction in energy per unit mass. Despite these differences, all the measured properties of PSOME are within ASTM specifications, confirming its suitability as an alternative fuel for compression ignition engines [45]. Due to its high ignition resistance, the product requires fewer safety precautions for storage and handling. Higher oil viscosity affects the atomization quality of isomethane fuel and increases BSFC in accordance with biodiesel investigations.

2.2. Cerium oxide (CeO_2) additive

Adding CeO_2 nano additives can improve combustion efficiency and reduce pollutants in biodiesel. Table 3 shows that CeO_2 nanoparticles (NPs) possess a variety of physicochemical properties [46], enabling applications at high temperatures, such as catalytic uses in fuel additives or thermal barrier coatings. CeO_2 exhibits excellent thermal stability, with a melting point of 2,400°C and a boiling point of 3,500°C, respectively. Its density of 7.215 g/cm^3 indicates a closely packed structure, identified as cubic (fluorite). The particles, generally less than 25 nm in diameter, have a high surface area-to-volume ratio, which contributes to their high reactivity in combustion environments. CeO_2 appears as a white to slightly yellowish powder that is mildly hygroscopic. Its water immiscibility ensures stability in the fueling system, and its oxygen buffering capability, due to its redox properties, can enhance burning efficiency and reduce emissions when used as a nano-additive.

To ensure stable dispersion of CeO_2 nanoparticles in the biodiesel–diesel mixtures, 0.1 wt% of Span-80 nonionic surfactant was added before sonication. The blends were ultrasonically agitated using a probe sonicator operating at 20 kHz and 500 W for 30 min to achieve uniform dispersion. The prepared samples were stored in sealed glass containers and monitored for 72 h with no visible sedimentation. The zeta potential measured for the optimized B30 + 50 ppm CeO_2 blend was –38.2 mV, confirming excellent colloidal stability. These steps ensured homogeneity and prevented nanoparticle agglomeration during engine testing.

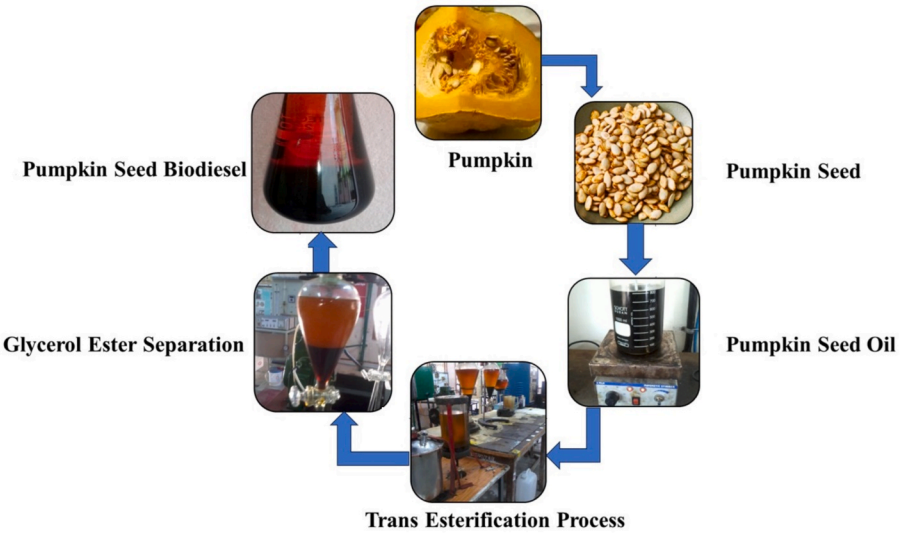

Fig. 1. Production of pumpkin seed biodiesel.

Table 2
Properties of Pumpkin Seed Biodiesel (PSOME).

Property	Diesel	Pumpkin seed biodiesel (B100)	ASTM Standards
Density (kg/m^3)	823.1	901.2	D 1298
Kinematic viscosity at 40°C (cSt)	3.9	5.8	D 445
Flash point (°C)	57	174	D 93
Gross calorific value (MJ/kg)	43.4	40.3	D 240
Fire point (°C)	69	190.2	D 93

Table 3
Physicochemical properties of cerium oxide.

Properties	Values
Molecular formula	CeO_2
Molar mass	172.115 g/mol
Physical Appearance	White to pale yellow solid; slightly hygroscopic
Density	7.215 g/cm^3
Melting point	2,400°C
Boiling point	3,500°C
Water solubility	Insoluble
Average Particle Size	Less than 25 nm
Crystal structure	Cubic (Fluorite)

2.3. Thermal barrier coating (TBC)

The thermal insulating coating used in this study is a ceramic composite that protects vital engine parts, such as the piston head and cylinder bore, thereby reducing heat loss and increasing combustion temperature [47,48]. This coating primarily consists of YSZ, 94%, known for its low thermal conductivity, high melting point (2700°C), and excellent phase stability at elevated temperatures. The residual components include alumina (2%) and ceria (4%), which contribute to thermal-shock resistance and sintering stability [31]. The coating was applied using plasma spraying, resulting in a micro-porous structure that enhances heat insulation and provides a secure mechanical bond with the metallic base material. The coating thickness was maintained at 0.3 mm for the cylinder liner and 0.15 mm for the piston [37]. The integrity and durability of the composite TBC were evaluated both before and after engine testing to confirm its effectiveness in a high-temperature diesel environment. Figs. 2 and 3 indicate the stability of the coating, showing only slight peripheral cracking in the piston crown, with no substantial damage observed elsewhere, confirming the robustness of the TBC even under the two load conditions.

Fig. 2. Coated Engine Piston and Cylinder Liner.

Fig. 3. Coated Engine Piston and Cylinder Liner after 100 h of engine Operation.

2.4. Experimental setup

Fig. 4 shows the schematic diagram of the test engine experimental arrangement. The work was conducted on a single-cylinder, four-stroke, direct-injection, water-cooled diesel engine equipped with an eddy current dynamometer and a data acquisition system. The engine was connected to the eddy current dynamometer, which serves as the brake power. It operated with typical settings, including a fuel injection pressure of 215 bar, a fuel injection timing of 26° before top dead center, and a constant compression ratio of 17.5:1. Temperatures of the inlet manifold, outlet manifold, and cylinder wall were recorded using a

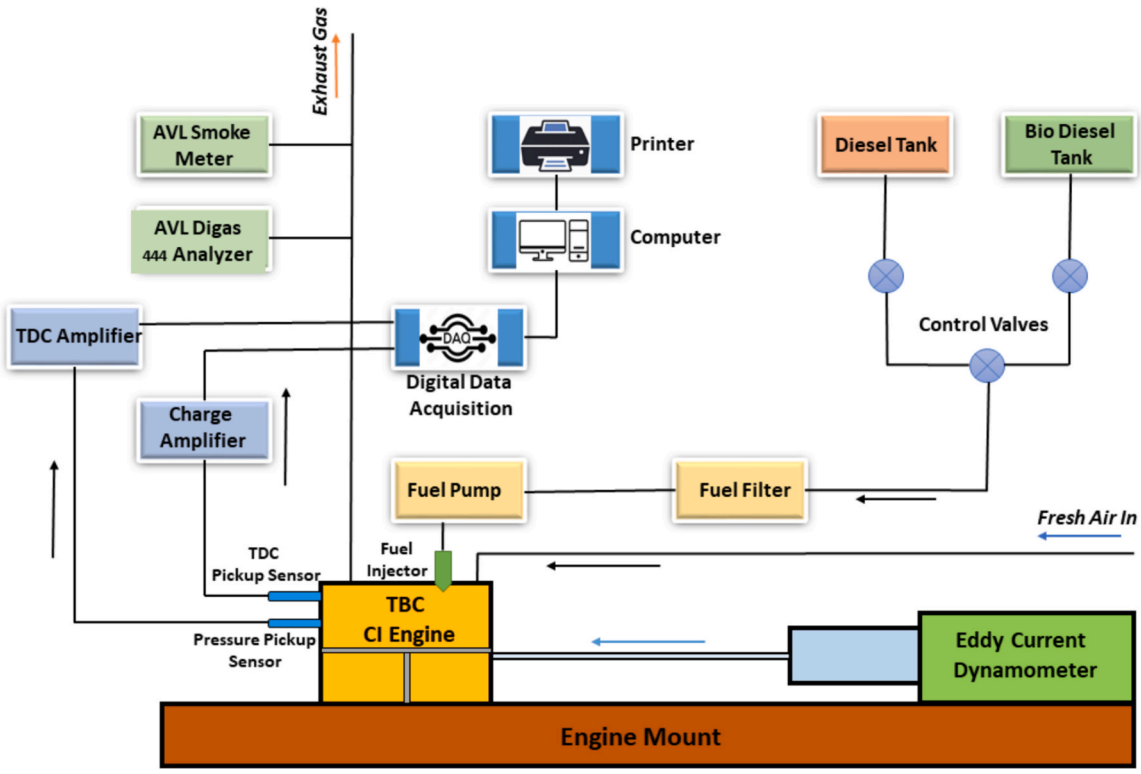

Fig. 4. Schematic Diagram of the Experimental Setup.

Chromel-Alumel thermocouple (type K) fitted at different locations. Engine exhaust emissions such as CO, HC, and NOx were measured using the NDIR (Non-dispersive infrared) technique of the AVL 444 di-gas analyzer. The smoke was evaluated in terms of smoke density using the Hartridge Smoke Unit (HSU) and was measured with the AVL 437C smoke meter. Table 4 presents the engine specifications.

2.5. Uncertainty analysis

The determination of uncertainty influenced the precursor, whose variance was generated during experimentation. Some criteria considered include environmental conditions, equipment, and reading observation calibration. The method of error propagation recommended by J. P. Holman [49] was used to establish the overall uncertainty in the experimental studies. Each experimental condition was repeated three times under identical operating parameters. The average of these repeated measurements was used to minimize random variations and improve data reliability (Table 5). The overall uncertainty was computed following Holman's root-sum-square method, and the total experimental uncertainty was estimated at ± 2.27%.

Table 4
Specification of the engine.

Specification	Details
Engine Type	Single-cylinder, 4-stroke, vertical, water-cooled CI engine
Manufacturer/Model	Kirloskar TV-1
Rated Power Output	5.2 kW at 1500 rpm
Operating Speed	1500 revolutions per minute (rpm)
Number of Cylinders	1
Stroke Cycle	Four-stroke
Compression Ratio	17.5:1
Cylinder Bore	87.5 mm
Stroke Length	110 mm
Ignition Method	Compression ignition

Table 5
Experimental Uncertainty.

Parameters	Range	Measuring technique	Accuracy	Errors (±)
Speed	0–10000 rpm	Principle of Magnetic pickup	±10 rpm	±0.1
Measurement of fuel flow	0–500 mm	Volume-based measurement	±0.1 cm^3	±1
Load	0–50 kg	Strain Gauge-Based Load Cell	±10 N	±0.2
Engine crank angle encoder	–	Principle of Magnetic pickup	±1 deg	±0.2
Temperature	0–1200°C	Temperature sensing thermocouple	±1 ∘C	±0.15
Time	–	Stop watch – Manual	±0.1 s	±0.2
Pressure	0–5000 psi	Principle of Magnetic pickup	±0.1 kg	±0.1
Deflection of manometer	0–250 mm	Balancing the Liquid Column	±1 mm	±1
NO	0–5000 ppm	Non-Dispersive Infrared (NDIR) Method	±12 ppm	±0.2
CO	0–10%vol.	Non-Dispersive Infrared (NDIR) Method	±0.02% volume	±0.2
Smoke	0–100 HSU	Opacimeter	±1 HSU	±1
HC	0–20000 ppm	Non-Dispersive Infrared (NDIR) Method	±10 ppm	±0.1

2.6. Experimental testing

Pumpkin seed biodiesel blends doped with CeO_2 nanoparticles were studied experimentally under various engine operating conditions to compare the performance and emission behaviors of the uncoated and coated compression ignition engines. The fuel types used for

examination were B10, B20, and B30, which contained 10%, 20%, and 30% of pumpkin seed biodiesel, respectively, mixed with standard diesel fuel. To enhance combustion efficiency, the nano-additive CeO_2 nanoparticles were incorporated at concentrations of 35, 45, and 55 ppm. Engine load was controlled at 50%, 75%, and 100% to simulate different operating conditions. The biodiesel/CeO_2 nanoparticles blends were sonicated for 30 min to achieve a homogeneous dispersion before testing. The engine was then run and allowed to reach a steady state for each test point. Under each condition, the engine was operated three times to collect performance characteristics and emissions data, which were averaged for analysis. Initial tests were conducted using the regular engine settings and untreated pistons and cylinder linings. Then, the solid piston top and cylinder liner were replaced with plasma-sprayed TBC to investigate their impact. A comparison of combustion and emission characteristics was performed for coated and uncoated engines with the nanoparticle-enhanced biodiesel blends and standard diesel. The physical integrity of the piston and cylinder liner was inspected after approximately 100 h of operation.

2.7. Machine learning prediction

In this paper, an ANN was used to simulate and predict the performance and emissions parameters of the engine using experimental data. The input parameters were the biodiesel blend percentage, engine load, and concentration of cerium oxide nanoparticles. The data were normalized and divided into training and testing datasets to construct predictive models. ANN regressor models were developed with a flexible topology that included hidden layers and neurons, optimized via a grid search under cross-validation to achieve the highest possible predictive performance [50]. The model training utilized the Adam optimizer with ReLU activation, and early stopping was implemented to avoid overfitting. Model performance was assessed using R^2, mean absolute error (MAE), and root mean squared error (RMSE). This machine learning method enabled both accurate and data-driven predictions of engine performance across a range of operating conditions.

2.8. Response surface Methodology (RSM)

The experimental data were processed and analyzed statistically using Response Surface Methodology (RSM) to optimize the response variables, including biodiesel composition, engine load, and CeO_2 nanoparticle content, with a focus on engine performance and emissions. An L27 orthogonal array was applied using a user-defined model in the Design Expert 13 software. This model was selected to ensure that all combinations of the factors, biodiesel blend (B10, B20, B30), engine load (50%, 75%, 100%), and CeO_2 nanoparticle concentration (35, 45, 55 ppm), were equally distributed across the 27 experimental runs. The L27 orthogonal array ensures that these combinations are systematically chosen to provide a comprehensive evaluation of the interactions and main effects while minimizing experimental runs. Quadratic polynomials were used as models to represent the nonlinear relationships between input factors and output responses. Model fitness was evaluated using Analysis of Variance (ANOVA) and residual diagnostics. The response surfaces generated from these models allowed the identification of the interactions among the system factors, enabling the determination of optimal operating conditions for achieving maximum engine performance and minimum emissions. This approach is particularly suitable for multi-response optimization in complex combustion systems.

In this study, the ANN and RSM methods were used in a complementary rather than comparative manner. The RSM model, based on a user-defined L27 orthogonal array, was utilized to perform multi-response optimization of the experimental factors (biodiesel blend, engine load, and CeO_2 concentration) and to identify the optimal combination of parameters that maximizes BTE while minimizing SFC and emissions. In contrast, the Artificial Neural Network (ANN) was trained using the experimentally obtained data and subsequently employed to predict engine performance and emissions for input conditions not included in the design matrix. Therefore, RSM served as a design-and-optimization tool, while ANN functioned as a predictive tool, enabling interpolation beyond the tested combinations. This integrated use of ANN for prediction and RSM for optimization strengthens the robustness of the analysis by combining statistically optimized experimental design with machine-learning-based generalization capability.

3. Results and discussion

3.1. SEM and EDX analysis of coating samples

The SEM image of the coating surface before combustion, shown in Fig. 5(a), reveals a typical porous microstructure characteristic of plasma-sprayed ceramic coatings. The surface is relatively uniform, with pores and splats that promote thermal insulation by trapping air and reducing heat migration.

This structure is crucial for the coating's ability to withstand the high-temperature environment of the engine. The coating's adhesion to the substrate was also visually evaluated, with no signs of delamination or failure in the bonding layer at this stage, indicating good adhesion strength between the TBC and the underlying material. Fig. 5(b) shows the SEM analysis after continuous combustion testing. The coating displayed slightly increased surface roughness, with a limited crack pattern mainly confined to the coating's edges. These changes are expected after prolonged exposure to high combustion temperatures. Despite these minor morphological changes, the overall structure of the coating remained largely intact, with no significant spalling or severe degradation. This indicates that the coating maintains its thermal stability and integrity under the thermal stresses experienced during engine operation.

Fig. 5(c) shows the Energy Dispersive X-ray (EDX) elemental mapping and spectrum for the post-combustion coating surface. The EDX analysis confirmed the presence of key elements in the coating, such as zirconium (Zr), oxygen (O), aluminum (Al), silicon (Si), calcium (Ca), iron (Fe), and cerium (Ce). The zirconium peaks dominate the spectrum, consistent with the yttria-stabilized zirconia (YSZ) matrix, while the cerium peaks indicate the presence of CeO_2 nanoparticles. The homogeneous dispersion of these elements throughout the coating suggests efficient distribution of nanoparticles, which is essential for enhancing the coating's thermal insulation properties and long-term performance. The post-test SEM and EDX analyses verify the structural integrity and compositional stability of the TBC after exposure to high combustion temperatures. These findings are vital for confirming the coating's applicability in enhancing engine thermal efficiency and durability, particularly for biodiesel-fueled operations. The minor morphological changes observed in the coating after testing did not significantly impair its thermal barrier function or adhesion strength, indicating good performance under operational conditions.

3.2. FTIR analysis of thermal barrier coating (TBC) powder

The FTIR spectrum of the thermal barrier coating (TBC) powder provides essential insights into its chemical composition and molecular structure. As shown in Fig. 6, the spectrum reveals several distinct absorption bands corresponding to specific functional groups and bonding characteristics of the material. These peaks help identify the chemical environment of the TBC components. The well-defined peaks at 2923 cm^{-1}, 2853 cm^{-1}, and 2642 cm^{-1} correspond to the stretching modes of C–H bonds. These are typically associated with organic residues or adsorbed hydrocarbons on the surface of the powder. The presence of these peaks indicates the potential for organic contamination during the powder synthesis or coating application process. These organic components could affect the overall chemical reactivity and stability of the TBC. The peaks observed at 2324 cm^{-1}, 2286 cm^{-1}, 2157 cm^{-1}, 2162

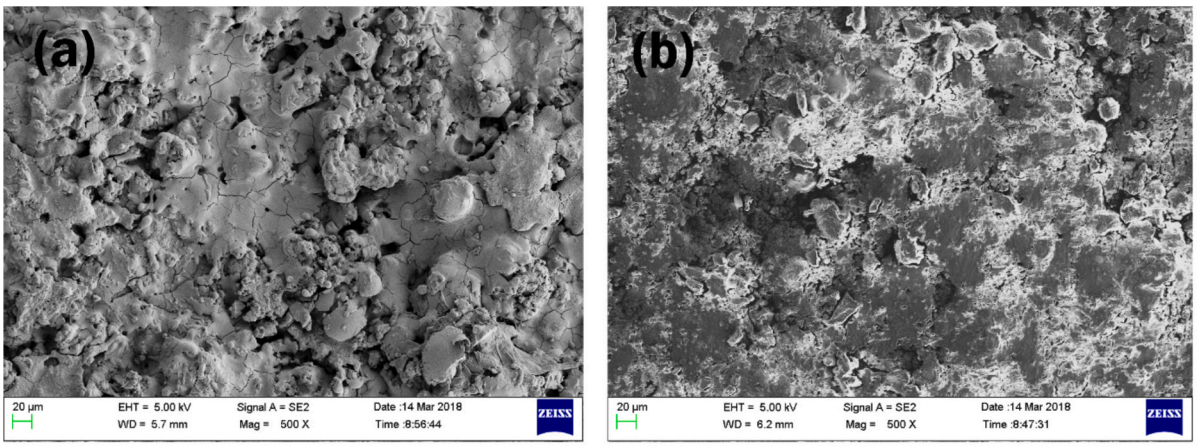

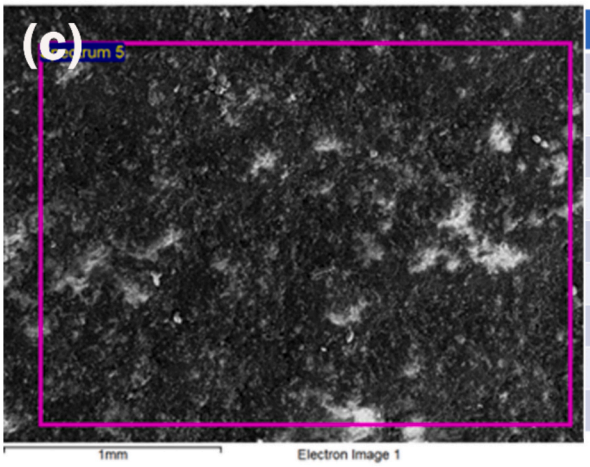

Element	Weight%	Atomic%
C K	70.57	84.90
O K	12.57	11.35
Al K	1.28	0.69
Si K	1.01	0.52
Ca K	0.61	0.22
Fe K	1.80	0.47
Zr L	10.86	1.72
Ce L	1.29	0.13
Totals	100.00	

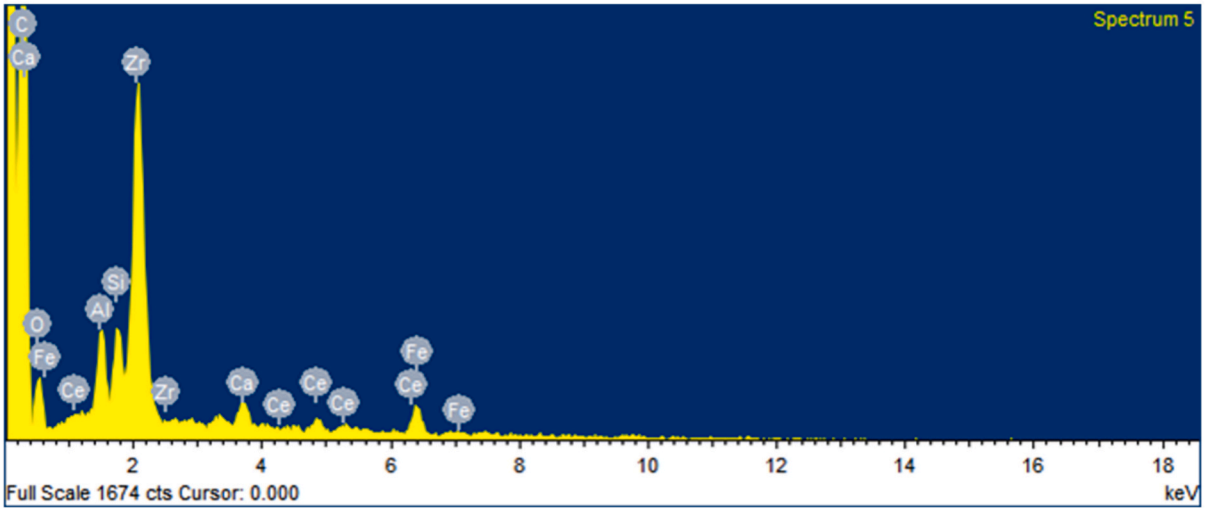

Fig. 5. SEM Image of Coated sample (a) before combustion (b) after combustion (c) EDX elemental mapping and spectrum of the post-combustion coating surface.

cm^{-1}, 2051 cm^{-1}, 2005 cm^{-1}, and 1981 cm^{-1} are attributed to carbonyl (C=O) stretching vibrations, suggesting the presence of carbonyl functional groups.

These may originate from slight organic contamination or residue from the synthesis process, indicating incomplete removal of organic substances during coating preparation. The presence of carbonyl groups can also provide insight into the thermal stability and potential for degradation of the TBC at high temperatures. A strong, broad absorption band at 875 cm^{-1} is observed, which is characteristic of metal–oxygen bonds. This peak corresponds to the ceramic components of the TBC, specifically yttria-stabilized zirconia (YSZ), alumina, and ceria. The presence of this peak is crucial as it indicates the ceramic nature of the TBC and reflects the thermal insulation properties of the material. The strength of this band suggests that the TBC powder retains its ceramic integrity, which is fundamental for its ability to withstand high temperatures in engine applications [51]. Overall, the FTIR spectrum confirms the chemical stability and soundness of the TBC powder, highlighting both the ceramic matrix and the minor presence of organic residues. These chemical characteristics are vital for assessing the thermal insulation performance of the coating, its ability to lower heat flux, and its durability under the high-temperature conditions encountered in the engine. The FTIR analysis, therefore, provides valuable

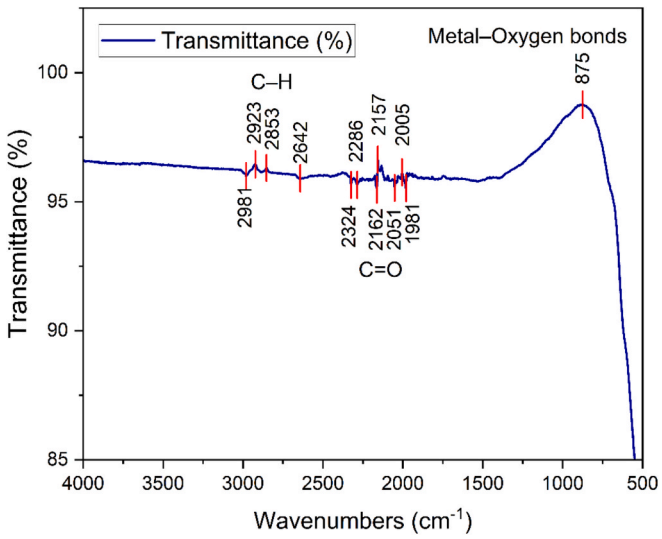

Fig. 6. FTIR Analysis of Thermal Barrier Coating (TBC) Powder.

information regarding the material's stability and potential performance in real-world applications.

3.3. Machine learning prediction performance

An ANN prediction model is developed in this paper to predict the performance and emissions of a CI engine using pumpkin seed biodiesel blended with cerium oxide nano additives in conjunction with a TBC engine. The ANN method was adopted because it is one of the most suitable tools for modeling complex nonlinear interactions among several input variables and target outputs, as is the case with the multifactorial engine system.

Data Preparation and Feature Selection: The input features for the model consisted of three significant experimental variables: biodiesel blend percentage, engine load percentage, and concentration of CeO_2 nanoparticles (CeO_2 ppm). These were selected due to their impact on combustion characteristics, thermal efficiency, and emissions. Before training, the input features were scaled using standard scaling to have a zero mean and unit variance, ensuring an equal contribution of each feature and speeding up the neural network convergence [52].

ANN Model Configuration and Data Preparation: The Artificial Neural Network (ANN) model was configured with an input layer containing three neurons, representing the three experimental input factors: biodiesel blend percentage, engine load percentage, and cerium oxide nanoparticle concentration (CeO_2 ppm). These parameters were chosen because they significantly influence combustion characteristics, thermal performance, and emissions. The ANN structure included one to three hidden layers, with the number of neurons in each hidden layer optimized using a grid search. The output layer contained a single neuron to predict the target parameter (such as SFC, BTE, CO, HC, NOx, etc.).

The dataset used for model training and testing consisted of 27 experimental runs, as shown in Table 6. 80% of the dataset (21 samples) was used for training, and 20% (6 samples) was reserved for testing and validation. This split ensured that a significant portion of the data was used to train the model, while the remaining 20% was utilized to test the model's performance on unseen data. The training set included combinations of biodiesel blends (B10, B20, B30), engine loads (50%, 75%, 100%), and CeO_2 concentrations (35, 45, 55 ppm), covering all factor levels in the design.

Before training, all input features were scaled to comparable ranges using a standard scaler, which balanced the contribution of each feature and enhanced the stability of the model's convergence during training. The model was trained for 1000 epochs in mini-batches of 4 samples. The network weights were optimized using the Adam optimizer, and the ReLU activation function was applied to introduce non-linearity in the hidden layers. Model performance was assessed using MSE and RMSE as loss functions to measure the accuracy and precision of the predictions.

Model Architecture and Training: A custom ANN regressor was built using the Custom KerasRegressor class, inheriting from scikit-learn's BaseEstimator and RegressorMixin. This design enables our API to integrate seamlessly into the scikit-learn pipeline and supports hyperparameter tuning through grid search. The ANN consists of a series of fully connected hidden layers, with the number of layers and neurons in each layer treated as tunable hyperparameters that will be optimized

Table 6
Experiment results of L27.

Exp No	Biodiesel Blend	Load %	CeO2 (ppm)	SFC (kg/kWh)	BTE (%)	CO (% of Volume)	HC (ppm)	Nox (ppm)	Smoke (HSU)
1	10	50	35	0.37	21	0.026	39	411	15
2	10	50	45	0.34	23	0.024	37	390	17
3	10	50	55	0.35	24	0.025	36	373	21
4	10	75	35	0.34	25	0.024	43	598	24
5	10	75	45	0.32	27	0.023	41	580	28
6	10	75	55	0.33	28	0.021	40	567	31
7	10	100	35	0.36	29	0.034	46	682	29
8	10	100	45	0.34	30	0.033	45	670	32
9	10	100	55	0.35	31	0.032	45	655	37
10	20	50	35	0.37	24	0.025	38	421	17
11	20	50	45	0.34	25	0.023	36	402	19
12	20	50	55	0.35	26	0.022	34	393	23
13	20	75	35	0.35	27	0.024	39	610	29
14	20	75	45	0.33	28	0.022	38	594	31
15	20	75	55	0.34	29	0.021	37	571	35
16	20	100	35	0.38	29	0.034	45	692	32
17	20	100	45	0.35	31	0.032	42	679	35
18	20	100	55	0.37	31	0.03	41	680	42
19	30	50	35	0.34	23	0.024	36	424	20
20	30	50	45	0.32	24	0.023	35	410	21
21	30	50	55	0.33	25	0.022	32	394	27
22	30	75	35	0.33	26	0.023	37	624	30
23	30	75	45	0.31	27	0.021	35	610	32
24	30	75	55	0.32	27	0.02	34	591	38
25	30	100	35	0.37	29	0.033	43	703	35
26	30	100	45	0.35	31	0.031	41	690	37
27	30	100	55	0.36	31	0.03	40	676	41

during the training process. The model was trained for over a thousand epochs, but early stopping was applied to prevent overfitting and enhance generalization. The output layer contains a single neuron to predict the continuous target variables.

Hyperparameter Optimization: ANNs were tuned by conducting a grid search on the number and size of hidden layers, varying from one to three hidden layers and from 2 to 8 neurons per layer. Following this systematic search, we selected the network design that yielded the highest coefficient of determination (R^2) on the training dataset, using three-fold cross-validation to ensure robustness and generalization. The results of hyperparameter optimization are provided in Table 7.

The best hyperparameter configurations for each ANN model are also visually presented in Fig. 7, illustrating the network architectures that delivered the highest predictive accuracy.

Model Evaluation and Performance: The optimized ANN models performed well in predicting all the target variables. In particular, the CO model exhibited an R^2 of approximately 0.99 on the validation set, demonstrating the successful capture of the complex, non-linear relationships among the various engine conditions. The corresponding MAE and RMSE values are both relatively small, indicating that the model has high precision and a minimal average deviation from the actual observations. Overall, these indices confirm that the ANN models are precise and reliable in predicting performance and emissions. The performance is detailed immediately after training is completed in Table 8.

Visualization and Interpretation: Plots of "actual versus predicted output" data points scatter around the identity line, showing a dense pattern along the line, which suggests that experimental values and predicted values are closely aligned, indicating strong predictive power of the model. Furthermore, the visualization of the training and validation loss curves showed smooth convergence without overfitting, as the validation loss line followed the trend of the training loss over epochs. The distribution of the actual and predicted SFC values was visualized using a density plot, which also confirmed the consistency of our model's predictive distribution. The obtained ANN model is a valuable tool for predicting and optimizing online engine performance characteristics under various operating conditions and fuel applications. This enables quick assessments of biodiesel blend performance and nano-additive effects without requiring multiple experiments, thereby saving time and cost. Additionally, the model's ability to provide accurate predictions of emissions is crucial for environmental impact assessments and the design of cleaner combustion concepts.

3.3.1. Machine learning model performance evaluation – training and validation loss plot

The performance of ANN models at both training and validation sets was extensively tested for each target variable after optimization. The training versus validation loss plots presented in Fig. 8 provide insight into how the RMSE evolves over 1000 epochs, offering clues about the model's learning dynamics and generalization.

The training RMSE consistently declined over the epochs for most of the targets, indicating successful learning. The RMSE across validation curves also exhibited a downward trend followed by a flattening response, indicating the learning curve of the models demonstrates sufficient generalization capability without severe overfitting. For example, in the SFC and BTE models, both training and validation RMSE errors decreased continuously, and the error floor leveled off at low error rates, suggesting that these models are robust in predicting samples. However, specific targets, including HC, NOx, and Smoke, exhibited larger oscillations in validation RMSE, potentially due to intrinsic variability in the emission measurements or more complex relationships. Nevertheless, the validation errors remained close to the training errors, indicating good generalization capability.

The R^2 ranged from 0.844 for SFC to 0.997 for NOx, indicating excellent predictability of engine performance and emission characteristics using the artificial neural network models. The MAE and RMSE values are also low, with an MAE of 0.0055 and an RMSE of 0.0065 for SFC, demonstrating minimal average prediction errors. This accuracy confirms the ANN's ability to accurately model complex nonlinear relations in engine dynamics. Overall, the trends of convergence in the loss curves, combined with the desirable error metrics, demonstrate the promising nature of the ANN models in predicting the performance and emission characteristics of a diesel engine fueled by PSB biodiesel in a thermal barrier coating environment with nano-additives. These findings support the use of the ANN machine learning method as a potentially reliable model for analyzing and predicting emissions based on engine parameters.

Table 7
Hyperparameter optimization result.

ANN Model	Number of Hidden Layers	Number of Neurons	R^2
SFC	3	6,5,5	0.844
BTE	3	8,6,4	0.946
CO	3	5,5,3	0.992
HC	2	8,6	0.95
Nox	3	6,6,3	0.997
Smoke	2	8,8	0.992

3.3.2. Actual vs. predicted performance of ANN models

The accuracy and generalization capability of the trained ANN models were demonstrated by plotting the experimental responses against the predicted responses for individual output parameters in Fig. 9. For each of the six predictors, the data points cluster along the ideal diagonal line with minimal dispersion, indicating high concordance between prediction and observation. The R^2 is displayed on the plots to suggest the predictive power of the models. The NOx showed the highest precision, with an R^2 value of 0.997, indicating an excellent match and implying that the model would accurately predict everything. The models for CO and Smoke also had very high R^2 values: 0.992 and 0.9924, respectively, demonstrating accurate model prediction of the emission parameters.

The BTE and HC models also performed well, with R^2 values of 0.946 and 0.9503, respectively. These findings suggest that the models effectively track the underlying trends in engine efficiency and unburnt hydrocarbon emissions. The SFC model, although slightly inferior ($R^2 = 0.844$), still demonstrated excellent predictive capability, as data points were closely aligned around the reference line. In each subplot, the red regression line and shaded confidence band further confirm a strong correlation between predicted and actual values, with slight variance. These graphics validate that the trained ANN models will enable accurate and consistent predictions of engine performance across diverse biodiesel blends, engine loads, and nanoparticle concentrations, thereby facilitating the optimization of performance and the forecasting of emissions in a diesel engine study. The ANN model performance was evaluated using both training and test datasets. While the training accuracy remained high ($R^2 > 0.99$), the test-set R^2 values ranged between 0.94 and 0.98 across the performance and emission outputs, indicating strong predictive capability and confirming that the network generalized well to unseen conditions. The close agreement between experimental observations and ANN predictions demonstrates that the model is robust and not overfitted.

3.3.3. Density plot analysis of actual vs. predicted values

The distribution of experimental data is visually compared with the corresponding predictions obtained from the ANN models for all the output parameters in the density plots (Fig. 10).

It is clear from the graph that the blue and red lines, representing the actual and predicted values, do not exhibit a significant gap between them, indicating that the models can effectively capture the underlying patterns of the data. Such a close relationship implies that the ANN models can emulate not only individual observations, but also the

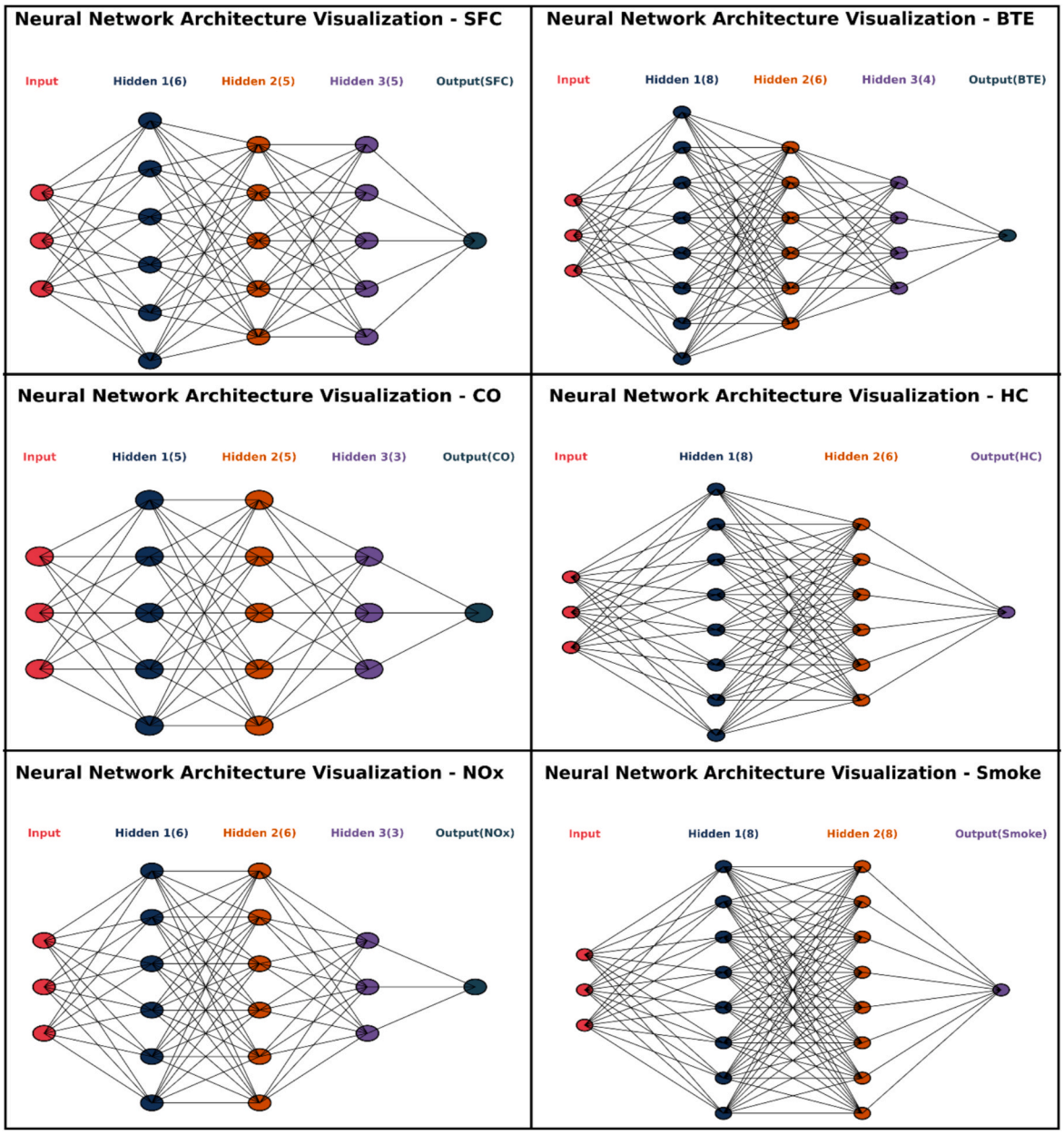

Fig. 7. The ANN architectures that delivered the highest predictive accuracy.

Table 8
Model performance after training.

ANN Model	MAE	RMSE	R^2
SFC	0.0055	0.0065	0.844
BTE	0.5704	0.7238	0.9458
CO	0.0003	0.0003	0.9919
HC	0.6202	0.7366	0.9503
NOx	4.7517	5.5760	0.9974
Smoke	0.6299	0.6881	0.9924

general trend and spread of the engine's performance and emission behaviour. This alignment in the probability density functions illustrates the robustness of the models. It validates their capability for accurately representing the complex and nonlinear nature of the combustion process, which is influenced by biodiesel blending, nanoadditives, and thermal barrier coatings, respectively.

3.4. Response surface methodology (RSM) optimization

After establishing predictive ANN models, additional optimization of the experimental data was conducted using RSM, developed with the assistance of the Design-Expert software package (version 13.0). An L27 orthogonal array design method was employed to systematically investigate the influence of process parameters on engine performance and emissions parameters. The goal of this optimization was to improve the BTE, SFC, CO, HC, NOx, and smoke emissions. Since the experimental responses were nonlinear, quadratic models were utilized to represent all potential complex interactions of these coupled variables. The quality and significance of these models were rigorously confirmed by analysis of variance (ANOVA). Three-dimensional surface plots were also created to provide a visual interpretation of interaction effects and to reveal the most favorable operational conditions for enhancing engine performance and reducing emissions. Such a method offers a powerful statistical tool for optimizing multidimensional experimental processes in combustion studies.

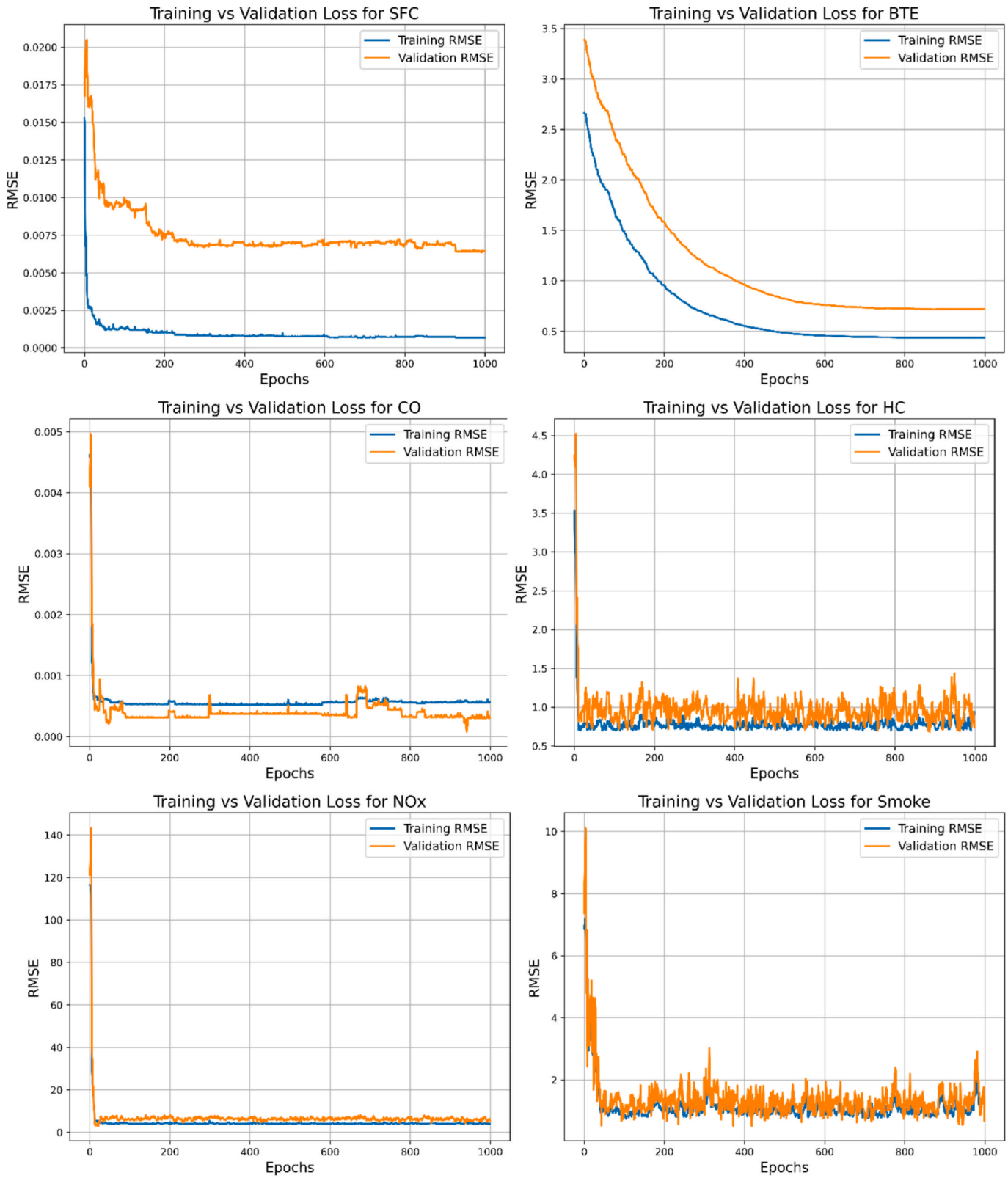

Fig. 8. Model Performance Evaluation – Training and Validation Loss Plot.

3.4.1. ANOVA analysis for model evaluation

The significance and appeal of the fitted quadratic models derived for engine performance and emissions were rigorously tested through Analysis of Variance (ANOVA). The ANOVA results (Tables in the supplementary file), reported for all models of SFC, BTE, CO, HC, NOx, and smoke opacity, reveal that all models are statistically significant, with p-values < 0.0001 for the overall models, reflecting robust model fits.

The leading contributing factors and their interactions are identified for each output parameter through the analysis of variance (ANOVA) tables. For example, engine load (Factor B) is consistently the strongest

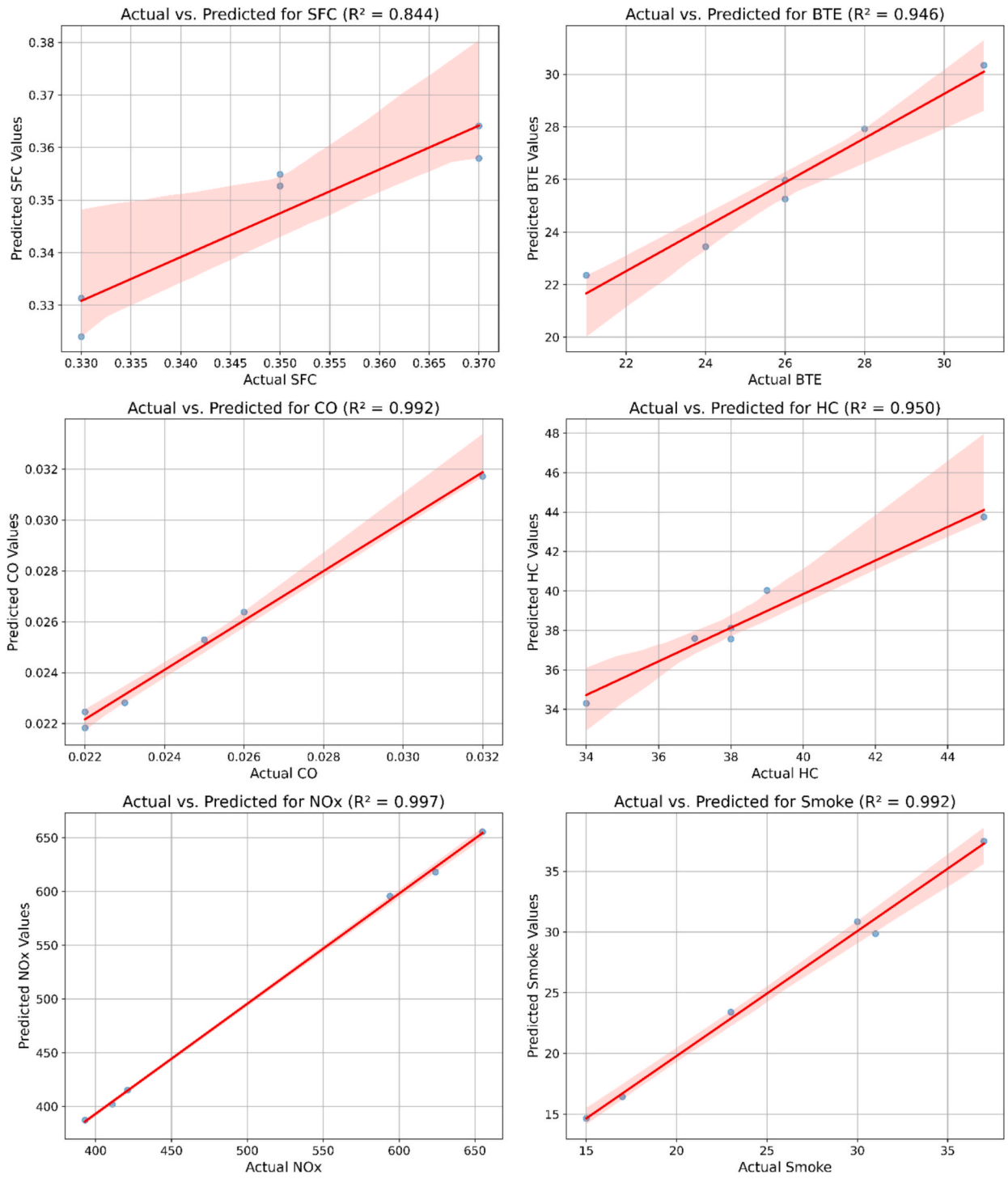

Fig. 9. Actual versus Predicted plot for each output parameter.

factor across all models, explaining 85% of the variance in BTE, NOx emissions, and other outputs. The bio-diesel proportion (Factor A) and the CeO_2 nanoparticle concentration (Factor C) also influence responses, though the extent of change varies based on the specific quantity involved. The second-order terms (squared factors A^2, B^2, C^2) are significant for most models, highlighting the nonlinear behavior of combustion influenced by fuel blend and nanoparticle additives. Interaction coefficients were substantial for factors such as AB (blend × load), indicating synergistic effects on fuel consumption.

The R^2 values of the models are close to 0.995, while adjusted R^2 values are similar, reflecting high explanatory power and low noise interference. A low coefficient of variation (C.V. %) for the models demonstrates precision and repeatability in both experimental and modeling procedures. Moreover, the sufficient precision ratio (greater than 4) indicates a suitable signal-to-noise ratio, implying that the models are applicable for navigating the design space. Overall, the ANOVA shows that the RSM second-order models are both statistically significant and reliable in predicting and optimizing the performance and emission characteristics of rock oil organoethallic nano-lubricant as a function of the two-way interactions between bio-diesel blend, engine load, and nano-additive concentration. The full ANOVA tables are provided in the supplementary information for reference.

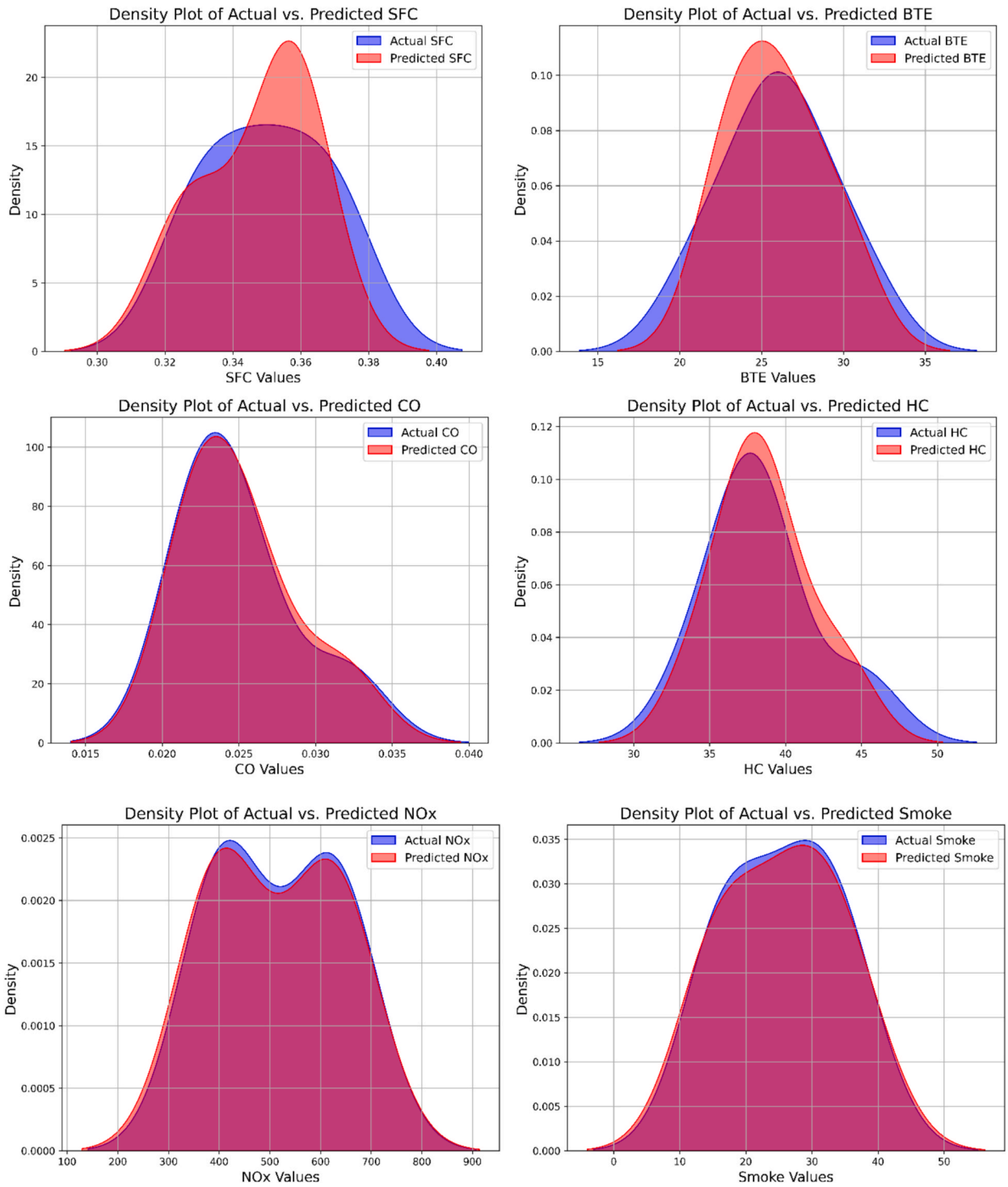

Fig. 10. Density Plot Analysis of Actual vs. Predicted Values.

3.4.2. 3D response surface and residual analysis for output model

The response surface plots generated by the RSM quadratic model for the SFC, illustrating the combination of critical input parameters affecting the SFC values, are presented in Fig. 11. The smooth curves on the plots indicate non-linear relationships and interactions between the fuel consumption-related variables.

In Fig. 11(a), the interaction between BDB and load is illustrated, indicating that SFC tends to decrease with an increase in load for different BDB levels. However, the effect of BDB is influenced by the level of load, revealing intricate behavior. It can be observed from Fig. 11(b) that the SFC decreases with increasing concentrations of CeO_2 at medium biodiesel percentages, which may suggest better combustion efficiency of nanoparticle additives. The same trend is also observed in Fig. 11(c), where both load and CeO_2 dosage may influence the reduction of SFC. The contour plots below each surface also clarify the optimal regions for fuel savings. The externally studentized residuals versus the experimental run order are presented in Fig. 11(d) and serve as a diagnostic tool to check the goodness of fit and the random pattern of residuals from the model. The residuals were randomly scattered within the control limits (±3.7226), with no apparent pattern and no signs of

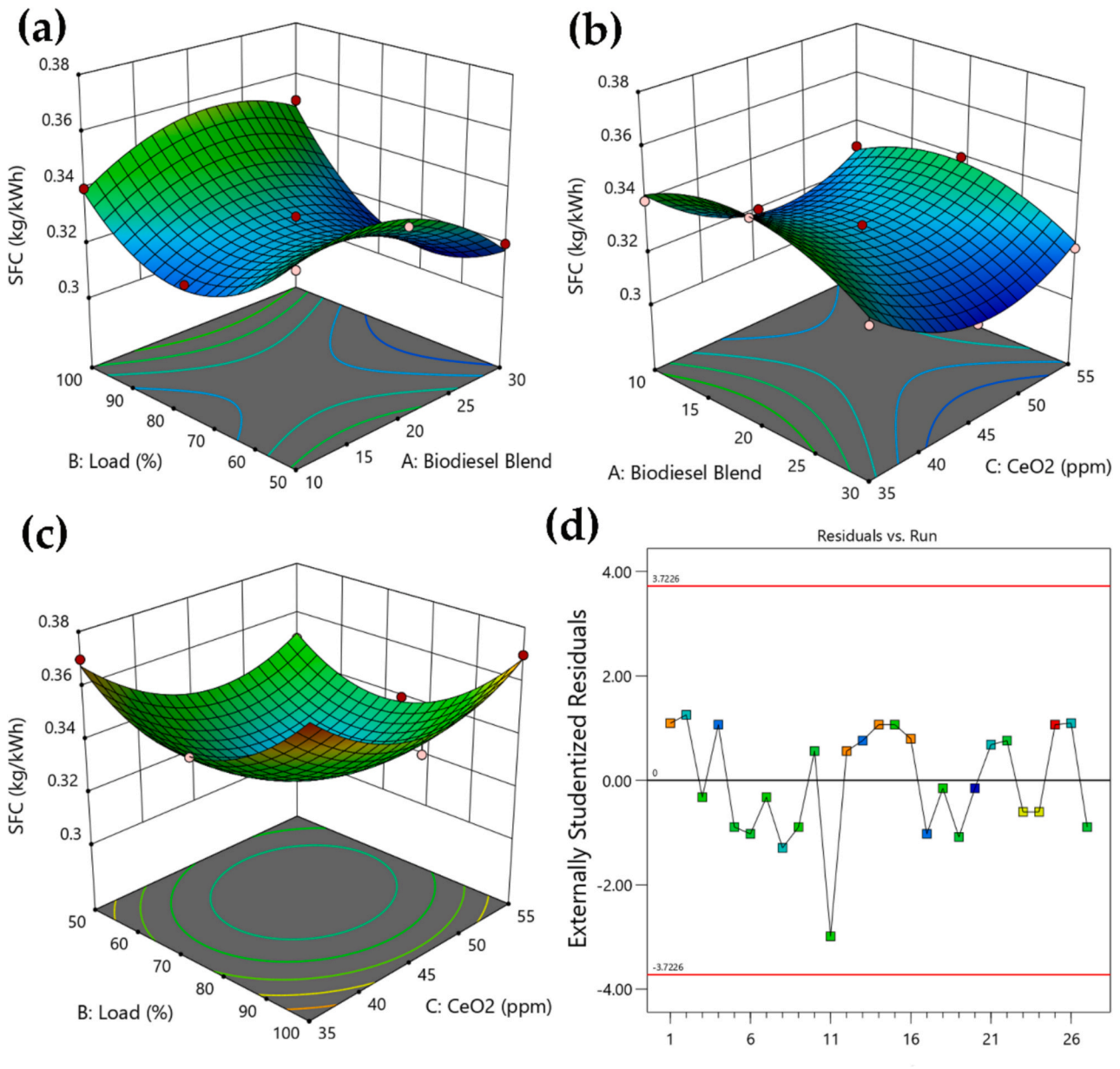

Fig. 11. 3D response surface (a-c) and Residual analysis (d) for the SFC model.

systematic error or outliers, demonstrating that the quadratic model is a good fit for the data. This residual behavior confirms the homoscedasticity and independence assumptions and supports the accuracy of the RSM model in forecasting SFC under different experimental conditions. All the plots further confirm that the developed RSM model is an effective tool for understanding the complex interactions of biodiesel blends, engine load, and CeO_2 nanoparticles, and that the SFC of coated CI engines can be accurately optimized.

3D response surface plots and residual diagrams for the brake thermal efficiency (BTE) model are shown in Fig. 12. In Fig. 12(a), the surface response plot illustrates the relationship between engine load, percentage of biodiesel blend, and BTE. The analysis indicates that a high engine load leads to higher brake thermal efficiency, and the relationship between load and BTE is direct. The variation of BTE with the blended proportion of biodiesel is nonlinear; BTE is higher with moderate biodiesel blends than with extremes, suggesting a threshold proportion of blend that maximizes thermal efficiency. This interaction is further demonstrated by the contour plotted in the lower panel, which indicates a ridge where BTE is maximized. In Fig. 12(b), the effect of the biodiesel blend and the addition of cerium oxide (CeO_2) nanoparticles on BTE is considered simultaneously. The plot reveals a synergistic performance where, at an optimum blend ratio, higher nanoparticle concentration induces more efficient combustion, thus increasing BTE. This smooth curvature suggests the quadratic nature of the model and its ability to capture complex nonlinear interactions. Fig. 12(c) focuses on the effects of engine load and CeO_2 concentration, showing that BTE is favorably enhanced with increased load and with moderate to high nanoparticle concentrations. This implies that combustion properties improve with nanoparticle additives, particularly under higher load conditions. Fig. 12(d) presents the externally studentized residuals against run order. The residuals are spread randomly across values between the control limits, without any clear systematic pattern or outliers, verifying that the homoscedasticity and independence conditions of the model are met. This confirms that the quadratic model is adequate and satisfactory for predicting BTE across the experimental range. Overall, these plots provide evidence that the model can capture the complex phenomena affecting BTE and thus can effectively optimize engine performance parameters.

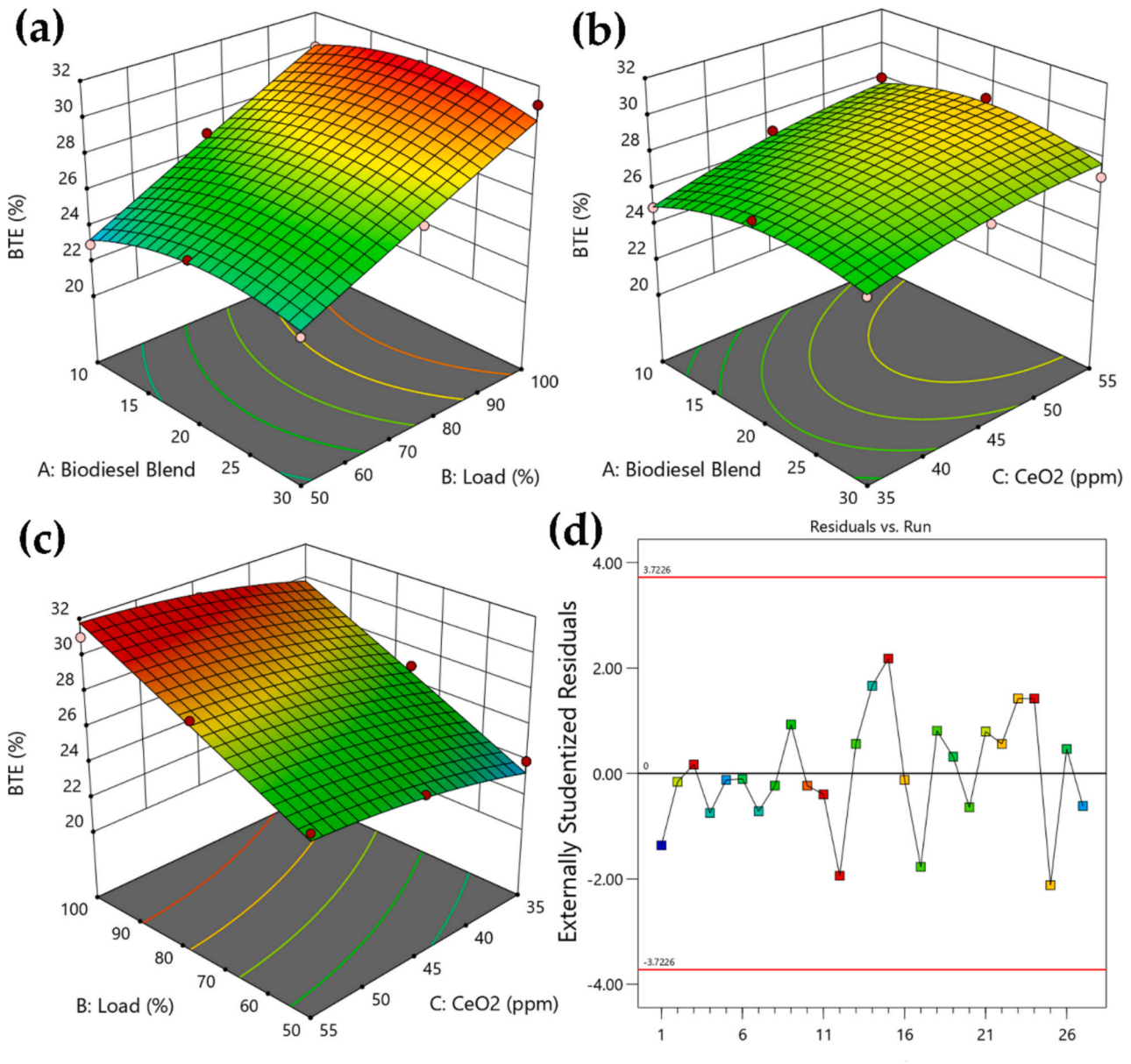

Fig. 12. 3D response surface (a-c) and Residual analysis (d) for the BTE model.

3D response surface plots for CO emissions: The contour plots of the three-dimensional response surface were created to illustrate the effects of biodiesel blend ratio, engine load, and CeO_2 nanoparticle loading on CO emissions, as shown in Fig. 13. The overall effects of the variable pairs on CO emission levels are demonstrated in Fig. 13(a), (b), and (c). Generally, CO emissions decrease with an increase in engine load and nanoparticle concentration, indicating improved combustion efficiency. It is also noted that CO emissions about the biodiesel blend percentage do not follow a linear relationship; instead, a specific optimum blend ratio exists at which emissions are minimized. The contour projection indicates the optimal zones for reduced CO emissions. Fig. 13(d) presents externally studentized residuals against run order, which shows that the random scatter within control limits indicates the model is statistically adequate and does not contain any significant outliers or patterns. These results verify the strength and consistency of the quadratic model in representing the complex interactions of factors affecting CO emissions in biodiesel-blended nano-diesel coated engines.

3D response surface plots for the interactions between biodiesel blend percentage, engine load, and the concentration of CeO_2 nanoparticles on HC emissions are shown in Fig. 14. The joint effect of two variables on HC is illustrated in Fig. 14(a), (b), and (c). The surfaces also indicate that HC emissions generally decrease with increasing engine load, suggesting more complete combustion occurs at higher loads. Biodiesel blend has exhibited a non-linear trend, with lower blends further exacerbating HC emissions. The presence of CeO_2 nanoparticles also helps reduce HC emissions, particularly at high-load modes, due to their catalytic influence on combustion. The contour plots beneath each surface help identify the optimal operating conditions for reducing HC emissions. Fig. 14(d) presents the externally standardized residuals versus run number, which fluctuate erratically within control limits, indicating no evidence of significant systematic errors or outliers. The randomness confirms the validity of the quadratic model and its strong predictive ability for HC emissions under varying experimental conditions. Overall, the figure illustrates the model's ability to predict nonlinear effects on HC emissions in the coated engine operating on biodiesel and nanoadditives.

Fig. 15 displays the response surface graphs in 3-D, illustrating the interactive effects of biodiesel blend percentage, engine load, and the

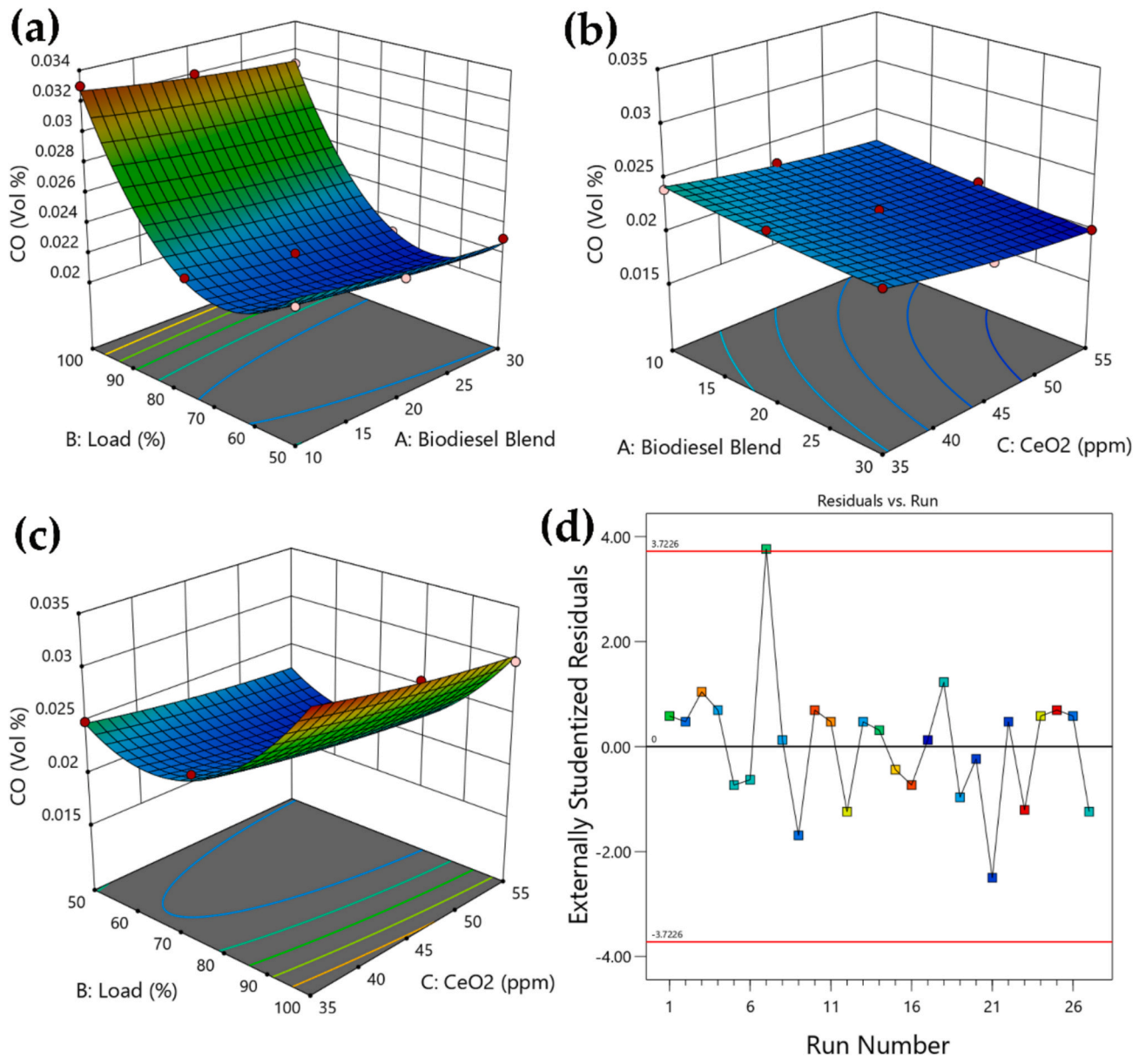

Fig. 13. 3D response surface (a-c) and Residual analysis (d) for CO model.

addition of cerium oxide (CeO_2) nanoparticles on NOx emissions. The interactions between these pairs of parameters are represented in Fig. 15 (a), (b), and (c), highlighting their effect on NOx levels. The surface maps indicate that NOx emissions tend to increase with higher engine loads due to greater combustion pressures and temperatures. The non-linear nature of the proportion of blended biodiesel modulates the formation of NOx. However, the CeO_2 nanoparticle shows a weaker than expected influence on NOx changes during the studied process. The contour plots complement the surface maps, illustrating the areas where NOx emissions increase or decrease as functions of various combinations of independent variables. The standardized residuals plotted against the experimental run order, along with the 95% control limits, are provided in Fig. 15(d). The residuals are randomly scattered within the control limits, indicating no significant lack of fit or outliers. This confirms that the quadratic model is adequate and suitable for predicting NOx emissions within the experimental range.

3D response surface diagram that illustrates the interactions among biodiesel blend ratio, engine load, and CeO_2 nanoparticle concentration on smoke emissions from the diesel engine. The pairwise interactions are presented in Fig. 16(a), (b), and (c). The plots indicate a general trend where smoke emissions decrease as engine load increases, reflecting improved combustion efficiencies at higher loads. Additionally, the biodiesel blends and the concentration of CeO_2 nanoparticles have a significant effect; increasing the concentration of CeO_2 reduces smoke opacity, suggesting a catalytic role for the nanoparticles in enhancing combustion. The contour projections provide further insight into the optimal combination of variables for minimizing smoke. Fig. 16(d) displays externally standardized residuals plotted against run number, revealing random scatter within the control limits. This randomness of residuals confirms the suitability of the quadratic form of the model and indicates the absence of outliers and patterns. Overall, the model accurately predicts the nonlinear interactions affecting smoke emissions, making it a valuable tool for optimizing engine performance.

The emission trends observed in this study can be explained through combustion thermodynamics. Carbon monoxide (CO) emissions are reduced due to the enhanced oxygen availability from biodiesel blends and CeO_2, which promote more complete combustion by increasing oxygen content and improving combustion efficiency. Similarly,

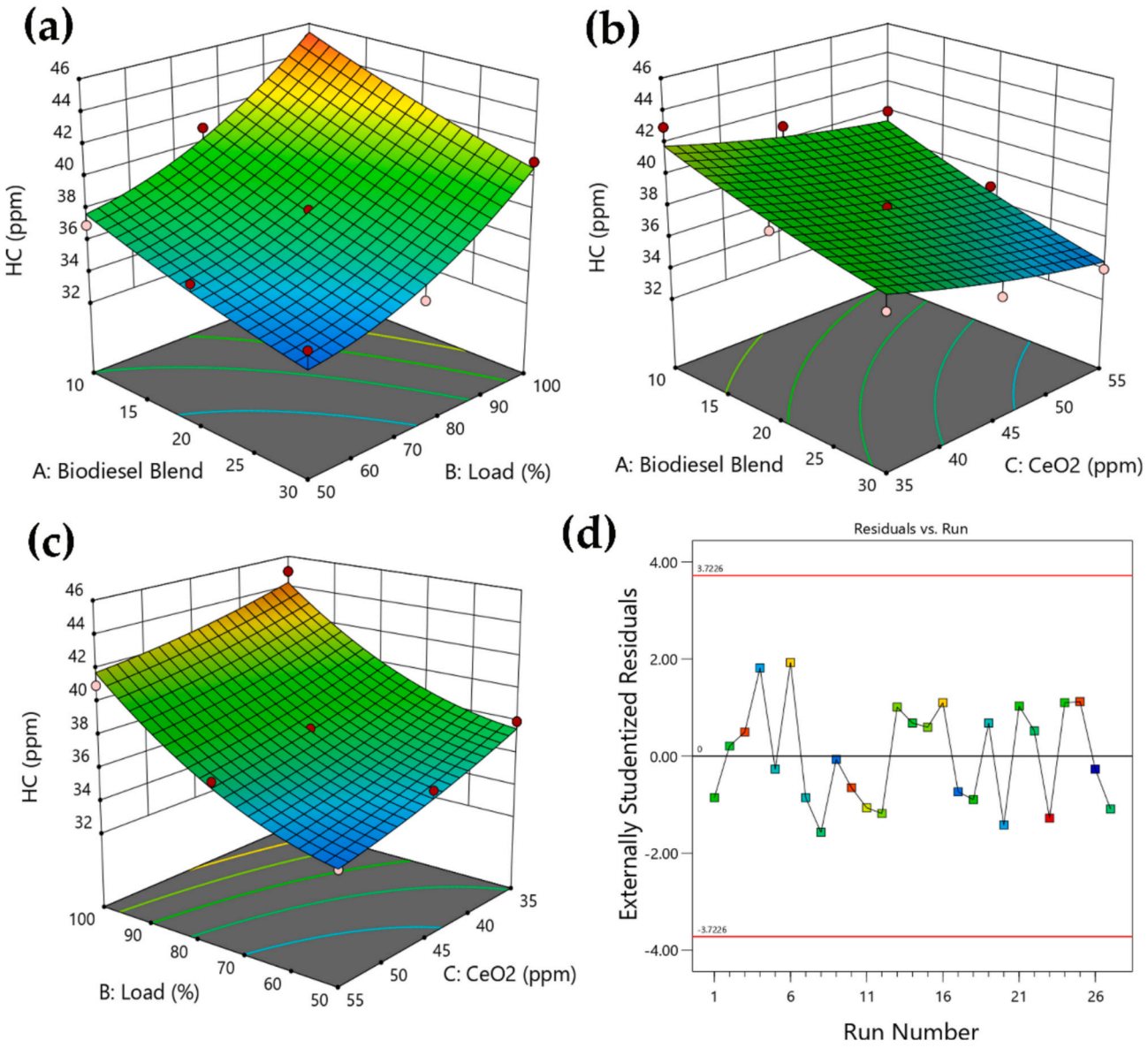

Fig. 14. 3D response surface (a-c) and Residual analysis (d) for the HC model.

hydrocarbon (HC) emissions decrease as the oxygenated nature of biodiesel and the oxygen-buffering effect of CeO_2 enhance fuel oxidation and combustion efficiency. However, the increase in nitrogen oxides (NOx) emissions can be attributed to the higher in-cylinder temperatures induced by CeO_2 nanoparticles, which accelerate combustion and promote the formation of NOx. In summary, while the combination of biodiesel and nano-additives improves combustion efficiency and reduces CO and HC emissions, it also results in a trade-off, with NOx emissions rising due to the elevated combustion temperatures.

Fig. 17 presents the actual vs. predicted plots for the RSM models for each of the response variables, including SFC, BTE, CO, HC, NOx, and Smoke. Each plot shows the relationship between the actual values obtained from the experiments and the predicted values generated by the model. The data points are clustered closely around the identity line, indicating a strong correlation between the actual and predicted values. This suggests that the RSM models are highly accurate in predicting the performance parameters across the different experimental conditions.

For SFC and BTE, the predicted values closely match the actual measurements, with very minimal deviation. Similarly, for CO, HC, NOx, and Smoke, the model predictions align well with the actual data, further validating the robustness of the RSM models. The color coding in the plots indicates the different levels of biodiesel blend and nanoparticle concentration, providing additional insight into the model's performance across various experimental settings. These plots reinforce the accuracy of the RSM models and their capability to predict engine performance and emissions effectively.

3.4.3. RSM optimization performance analysis

The optimization results based on Response Surface Methodology (RSM) are presented in Fig. 18. The study aimed to maximize the Brake Thermal Efficiency (BTE) while minimizing other output emissions, including Hydrocarbons (HC), Nitrogen Oxides (NOx), Carbon Monoxide (CO), and smoke. A desirability value of 1.000 was achieved, indicating an optimal balance between competing factors. The RSM optimization suggested that the ideal operating conditions for biodiesel performance and emission reduction were at a 30% biodiesel blend, 52% engine load, and a CeO_2 nanoparticle concentration of approximately 50 ppm.

Under optimal conditions, the Specific Fuel Consumption (SFC) decreased to 0.316 kg/kWh, showing improved fuel efficiency. The maximum Brake Thermal Efficiency (BTE) reached 24.87%, indicating higher energy conversion effectiveness. Emissions were notably

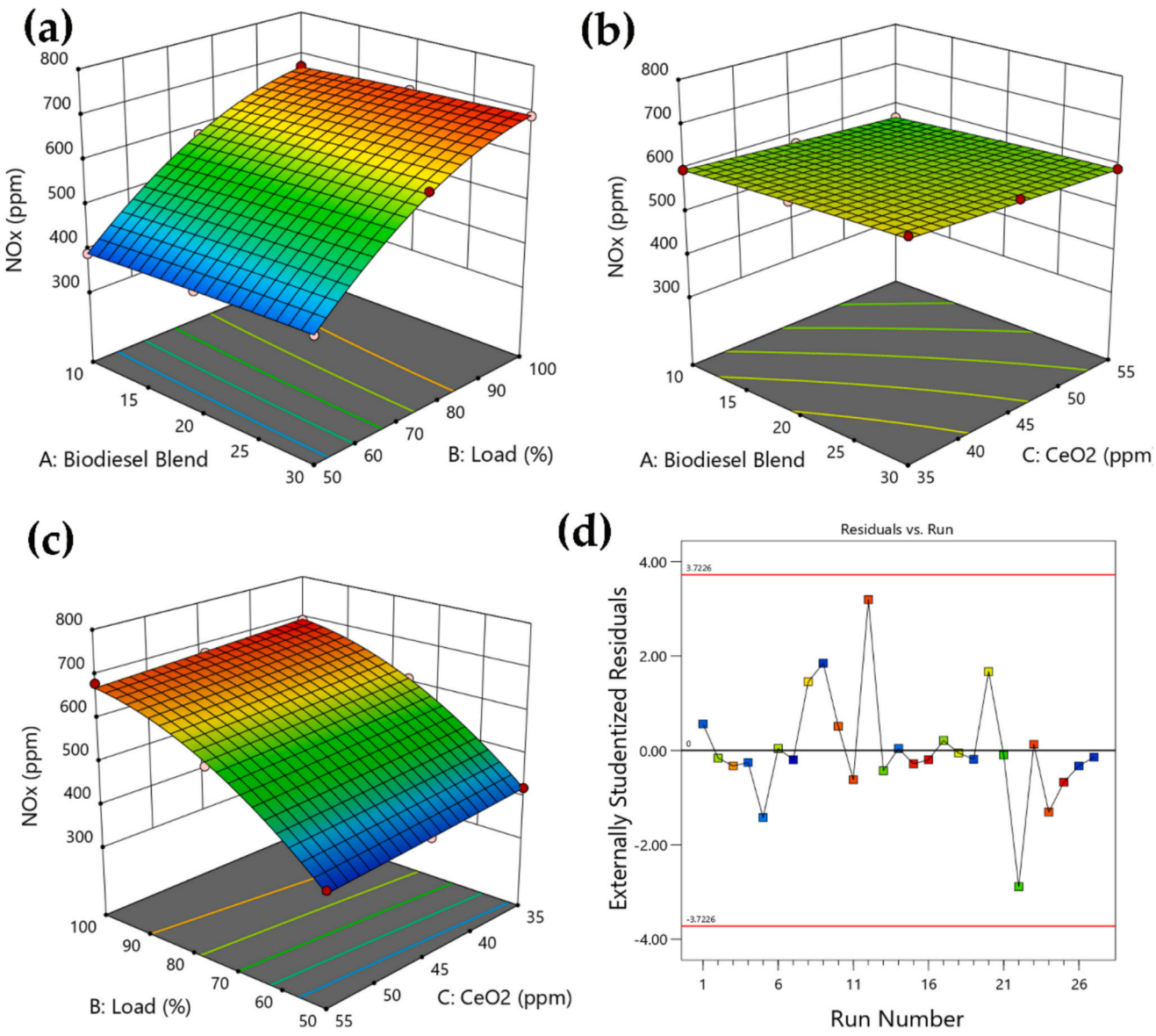

Fig. 15. 3D response surface (a-c) and Residual analysis (d) for the NOx model.

lowered, with CO reducing to 0.0217 vol%, HC to 33.06 ppm, NOx to 420.63 ppm, and smoke opacity to 24.38 HSU. To compare performance enhancements, the optimized operating condition (B30, 52% load, 50 ppm CeO_2) was assessed against the baseline diesel. The optimized blend resulted in a 12.5% increase in BTE (from 22.1% to 24.87%) and an 8.4% decrease in SFC (from 0.345 to 0.316 kg/kWh), as well as roughly 20% less CO, 30% less HC, and 25% less smoke opacity compared to baseline diesel. These findings confirm that combining pumpkin seed biodiesel, CeO_2 nanoparticles, and TBC improves combustion efficiency versus conventional diesel operation.

To further validate the effectiveness of the optimization, a comparison of the current results with existing literature is provided in Table 9. Several studies have explored the use of different biodiesel blends and nano-additives in engine performance, with varying results. For example, research by Vinothkannan et al. [53] showed a significant improvement in Brake Thermal Efficiency (BTE) and a reduction in CO and HC emissions when using a biodiesel blend with a nano-additive. In contrast, studies focused on conventional diesel engines and biodiesel blends without nano-additives showed less reduction in emissions and a marginal increase in BTE [40].

The current study's optimization of BTE and emissions performance using the 30% biodiesel blend, CeO_2 nanoparticles, and thermal barrier coatings aligns with these findings and extends the application of such additives to more sustainable biofuels, such as pumpkin seed biodiesel. This suggests the potential for improved engine performance and environmental impact in commercial applications.

3.5. *Experimental validation of optimization results*

To further validate the optimization results, the predicted optimum conditions (B30 biodiesel, 52% engine load, and 50 ppm CeO_2) were experimentally tested, and the results were compared with the ANN predictions. Table 10 presents the experimental validation of the optimized values for key engine parameters, including SFC, BTE, CO, HC, NOx, and Smoke, with the corresponding ANN predicted values. The predicted values align closely with the experimental results, confirming the accuracy of the optimization process and the applicability of the optimized conditions for improving engine performance.

Furthermore, Table 11 shows the percentage error between the experimental and ANN predicted values, indicating that the ANN model provides reliable predictions with minimal error. The percentage error for each parameter (SFC, BTE, CO, HC, NOx, and Smoke) is low,

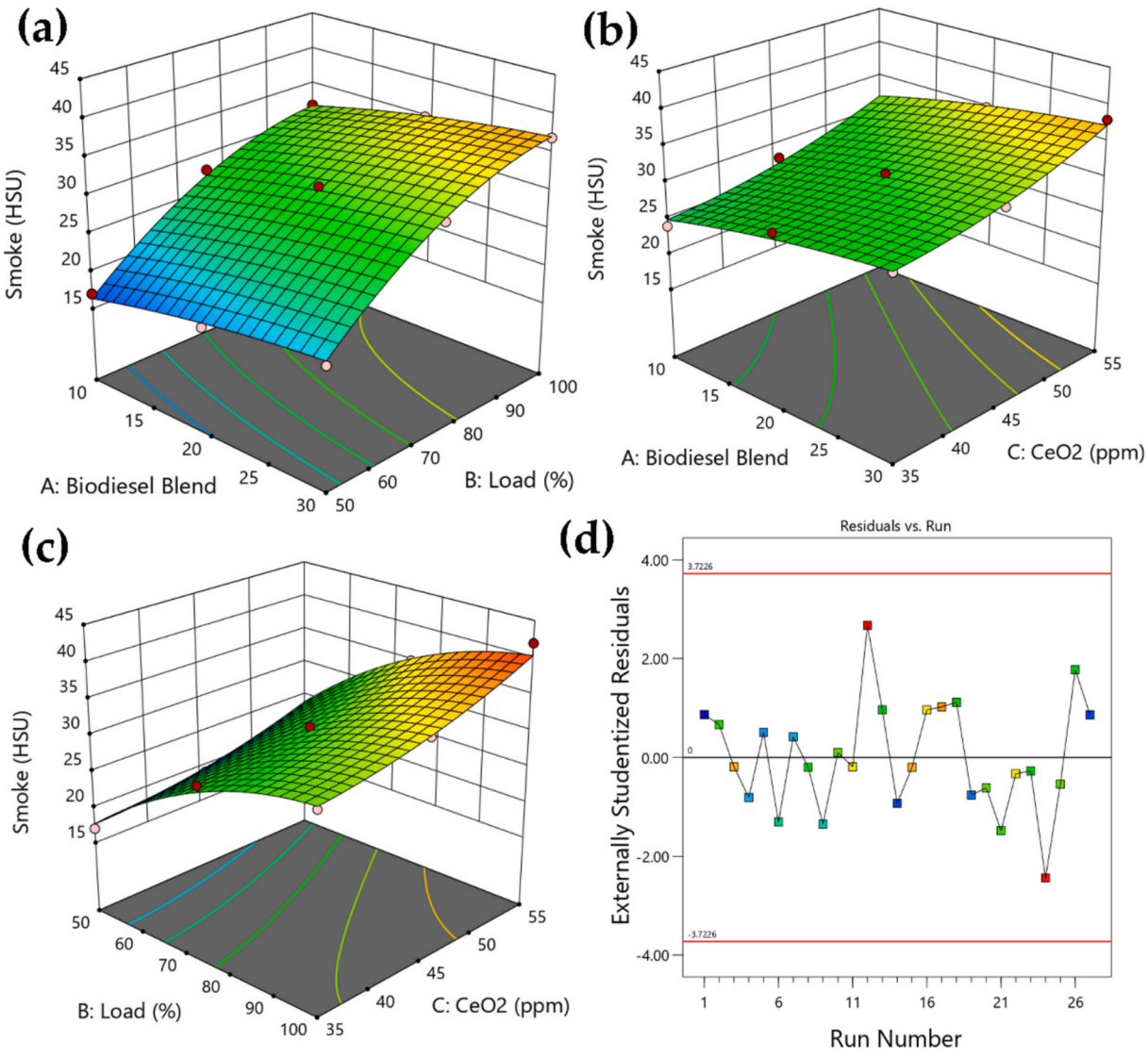

Fig. 16. 3D response surface (a-c) and Residual analysis (d) for Smoke model.

supporting the conclusion that the optimization process and the ANN model's predictions are robust and accurate.

These validation results further reinforce the effectiveness of the RSM-ANN approach in optimizing engine performance and minimizing emissions under real-world operating conditions. The close agreement between the predicted and experimental values demonstrates the potential of this combined approach for optimizing biodiesel-fueled CI engines.

4. Conclusions

This study investigated the impact of TBCs and eO_2 nano-additives on the performance and emission characteristics of pumpkin seed biodiesel in CI engines. The results demonstrated that combining advanced nanomaterial-based biodiesel with TBCs significantly improved combustion efficiency, leading to lower emissions and higher BTE. The optimization of operating conditions, such as a 30% biodiesel blend, 52% engine load, and 50 ppm CeO_2, resulted in the best performance, with reduced SFC, CO, HC, NOx, and smoke emissions, while maximizing BTE. SEM and EDX analyses confirmed the stability and durability of TBCs under high-temperature combustion conditions, with minimal degradation and uniform dispersion of CeO_2 nanoparticles.

The ANN model successfully predicted engine performance and emission parameters with high accuracy ($R^2 > 0.84$), demonstrating its potential as a real-time, data-driven tool for engine optimization. The study also employed RSM for multi-objective optimization, identifying optimal conditions for performance and emissions. Although the dataset consists of 27 samples, ANN was carefully trained using grid-search hyperparameter tuning and k-fold cross-validation to minimize overfitting. The model's purpose is limited to interpolation within the RSM design space, which is supported by several similar studies in biodiesel and nano-additive engine modeling. Coating longevity was not fully addressed, and further testing over extended operational periods is needed to assess the long-term durability of the TBCs. Additionally, while the ANN model showed promising prediction accuracy, real-world engine behavior under more variable conditions, such as different environmental factors, was not considered. Further work could also explore the effect of other nano-additives in combination with different biodiesel feedstocks to enhance fuel performance and emission reduction. Moreover, the study did not evaluate the potential economic viability of using pumpkin seed biodiesel and TBCs at a larger scale, which could be an important consideration for future studies.

This study demonstrates the strong potential of biofuel–nanomaterial synergy and establishes a useful framework for hybrid optimization approaches in cleaner engine design. While the findings show promising improvements in efficiency and emission

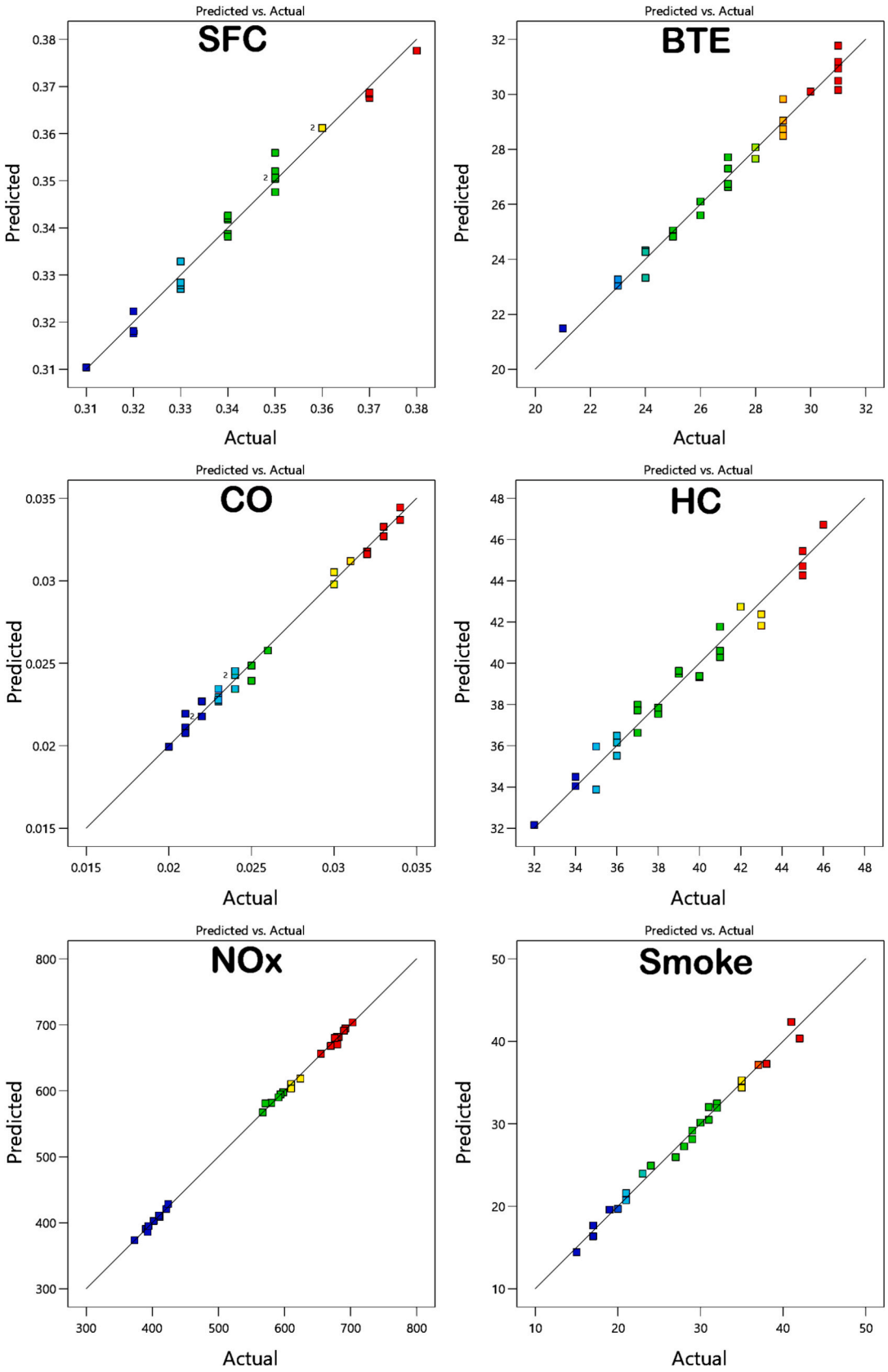

Fig. 17. Actual vs. Predicted Plots for RSM Analysis of Engine Performance and Emissions.

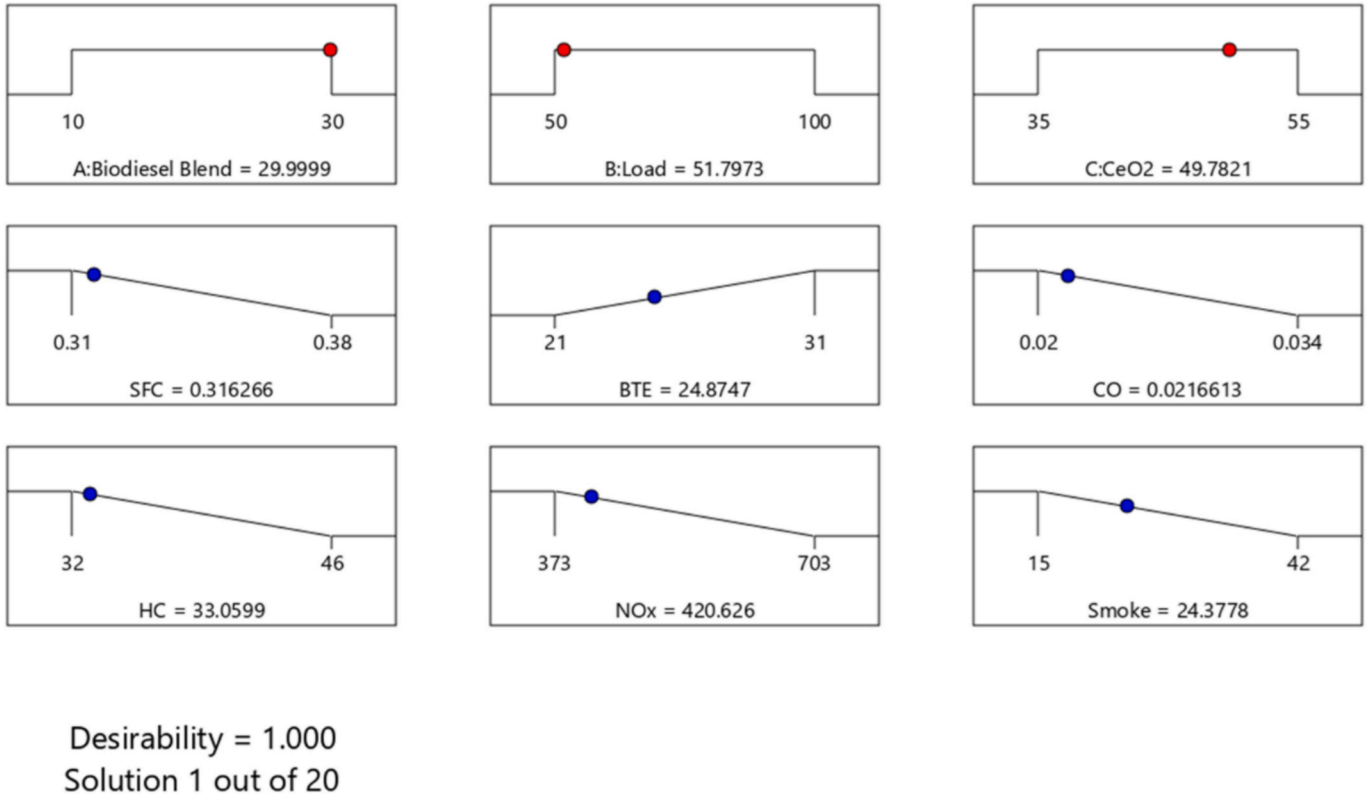

Fig. 18. The optimization results using RSM.

Table 9
Comparison of optimisation result with existing literature.

Study	Fuel Type	BTE Improvement	SFC Reduction	CO Reduction	HC Reduction	NOx Increase	Smoke Reduction
Current Study (Optimized RSM)	Pumpkin Seed Biodiesel + CeO_2	24.87%	0.316 kg/kWh	~20%	~30%	~18%	~25%
Kumaravel et al. [40]	Biodiesel + TBC + CeO_2	31.6%	13% lower	40%	15%	Increased	~14%
Vinothkannan & Pushparaj [53]	Pumpkin + Teak Biodiesel + DEE	35.5%	25.8% lower	26.67%	15%	Decreased	Lowered

Table 10
Experimental validation of optimum value with ANN.

Exp	Input Parameters			SFC		BTE		CO		HC		Nox		Smoke	
	Biodiesel Blend	Load %	CeO2 (ppm)	EXP	ANN	EXP	ANN	EXP	ANN	EXP	ANN	EXP	ANN	EXP	ANN
Optimum	30	52	50	0.32	0.31	24.87	25.06	0.02	0.02	33.05	33.10	420.62	432.55	24.38	25.32

Table 11
% of Error of Experimental value vs ANN prediction.

Exp	Input Parameters			% of Error					
	Biodiesel Blend	Load %	CeO2 (ppm)	SFC	BTE	CO	HC	Nox	Smoke
Optimum	30	52	50	-3.125	0.763	0.0	0.1512	2.83	3.85

reduction, further research is required to evaluate the long-term durability of thermal barrier–coated components under extended engine operation. Additionally, a life-cycle assessment (LCA) of nanoparticle production, disposal, and environmental footprint is essential to determine the real-world sustainability and viability of CeO_2-enhanced biodiesel systems. Such future investigations will help translate these laboratory-level advancements into robust, scalable solutions for green transportation technologies.

CRediT authorship contribution statement

V.S. Shaisundaram: Resources, Conceptualization. **Saravanakumar Sengottaiyan:** Writing – original draft, Project administration, Writing – original draft, Project administration. **R. Aruna:** Validation, Software. **R. Muraliraja:** Methodology, Investigation.

Funding

There are no funding sources for this research work.

Declaration of competing interest

The authors declare that they have no known competing financial interests or personal relationships that could have appeared to influence the work reported in this paper.

Appendix A. Supplementary data

Supplementary data to this article can be found online at https://doi.org/10.1016/j.fuel.2026.138434.

Data availability

Data will be made available on request.

References

[1] Imran S, Gul M, Kalam MA, Zulkifli NWM, Mujtaba MA, Yusoff MNAM, et al. Effect of various nanoparticle biodiesel blends on thermal efficiency and exhaust pollutants. Int J Energy Environ Eng 2023;14:937–48. https://doi.org/10.1007/s40095-023-00557-1.
[2] Gaddigoudar PS, Basavarajappa YH, Banapurmath NR, Harari PA. Effect of biogas flow rate on the combustion, emission and performance characteristics of dual fuel engine fuelled with ceiba pentandra biodiesel. Mater Today Proc 2023. https://doi.org/10.1016/j.matpr.2023.06.259.
[3] Gupta A, Kumar R, Maurya A, Ahmadi MH, Ongar B, Yegzekova A, et al. A comparative study of the impact on combustion and emission characteristics of nanoparticle-based fuel additives in the internal combustion engine. Energy Sci Eng 2024;12:284–303. https://doi.org/10.1002/ese3.1614.
[4] Khond VW, Kriplani VM. Effect of nanofluid additives on performances and emissions of emulsified diesel and biodiesel fueled stationary CI engine: a comprehensive review. Renew Sustain Energy Rev 2016;59:1338–48. https://doi.org/10.1016/j.rser.2016.01.051.
[5] Chen Y, Zhang J, Zhang Z, Zhang B, Hu J, Zhong W, et al. A comprehensive review of stability enhancement strategies for metal nanoparticle additions to diesel/biodiesel and their methods of reducing pollutant. Process Saf Environ Prot 2024;183:1258–82. https://doi.org/10.1016/j.psep.2024.01.052.
[6] Mofijur M, Ahmed SF, Ahmed B, Mehnaz T, Mehejabin F, Shome S, et al. Impact of nanoparticle-based fuel additives on biodiesel combustion: an analysis of fuel properties, engine performance, emissions, and combustion characteristics. Energy Convers Manag X 2024;21:100515. https://doi.org/10.1016/j.ecmx.2023.100515.
[7] Cuma MU, Koroglu T. A comprehensive review on estimation strategies used in hybrid and battery electric vehicles. Renew Sustain Energy Rev 2015;42:517–31. https://doi.org/10.1016/j.rser.2014.10.047.
[8] Chen H, Wang B, Huang Z. Greenhouse gas emission prediction and impact analysis of dual-fuel engine. Process Saf Environ Prot 2024;191:1–13. https://doi.org/10.1016/j.psep.2024.08.079.
[9] Ahmed MM, Pali HS, Khan MM. Feasibility of nanoparticles fused in biodiesel for CI engines: an integrated and historic review. vol. 149. Springer International Publishing; 2024. https://doi.org/10.1007/s10973-024-13147-y.
[10] Cs D, Devarajan Y. Performance and emission analysis of sterculia foetida biodiesel enhanced with butanol: Combustion efficiency and emission mitigation. Results Eng 2025;25:104586. https://doi.org/10.1016/j.rineng.2025.104586.
[11] Jamrozik A. Biodiesel/alcohol blends as fuel for compression ignition engines – a review. J Energy Inst 2025;121:102130. https://doi.org/10.1016/j.joei.2025.102130.
[12] Li J, Huang Z, Tao B, Sun X, Pan J. Effects of EGR rate and temperature on combustion and emissions characteristics of compression ignition engines fueled with hydrotreated vegetable oil. ACS Omega 2025. https://doi.org/10.1021/acsomega.4c08533.
[13] Sakthivel R, Ramesh K, Purnachandran R, Mohamed SP. A review on the properties, performance and emission aspects of the third generation biodiesels. Renew Sustain Energy Rev 2018;82:2970–92. https://doi.org/10.1016/j.rser.2017.10.037.
[14] Dubey A, Prasad RS, Kumar Singh J, Nayyar A. Optimization of diesel engine performance and emissions with biodiesel-diesel blends and EGR using response surface methodology (RSM). Clean Eng Technol 2022;8:100509. https://doi.org/10.1016/j.clet.2022.100509.
[15] Alterkaoui A, Belibagli P, Arslan H, Dizge N, Balakrishnan D. Heterogeneous catalyst production from waste cucumber stems and investigation of production potential in biodiesel. Process Saf Environ Prot 2025;196:106842. https://doi.org/10.1016/j.psep.2025.106842.
[16] Song Y, Li R, Qian Y, Zhang L, Wang Z, Liu S, et al. Study on spray characteristics of biodiesel alternative fuels for in-cylinder environment of diesel engine. J Energy Inst 2024;113:101507. https://doi.org/10.1016/j.joei.2023.101507.
[17] Natarajan U, Subramaniam RB. An experimental investigation on a CI engine with magnesium- doped zinc oxide nano-additives in fish oil biodiesel blends. J Therm Anal Calorim 2024;149:11793–805. https://doi.org/10.1007/s10973-024-13538-1.
[18] Kumar VD, Rajendran S, Hemadri VB, Prakash C, Sengottaiyan S. Experimental investigation of operating parameter effect on DI CI diesel engine using flamboyant biodiesel blends. Key Eng Mater 2024;1006:33–42. https://doi.org/10.4028/p-J7hz6w.
[19] Talesh Amiri S, Shafaghat R, Jahanian O, Alamian R. Experimental study on high fatty acid WCO biodiesel effects on RCCI engine performance, and emissions, considering fuel oxygen level. Biofuels 2025:1–9. https://doi.org/10.1080/17597269.2025.2450167.
[20] Zheng F, Cho HM. The Comprehensive Effects of Nano Additives on biodiesel Engines—A Review. Energies 2024;17. https://doi.org/10.3390/en17164126.
[21] Dinesh Kumar V, Mrityunjayaswamy KM, Chinnapandian M, Hemadri VB, Saravanakumar S. Comparison on the Combustion Characteristics of the Methyl Esters of Papaya Oil and Delonixregia Oil and Its Blends on Single Cylinder Diesel Engine BT - Recent Advances in Materials and Modern Manufacturing. In: Palani IA, Sathiya P, Palanisamy D, editors., Singapore: Springer Nature Singapore; 2022, p. 379–88.
[22] Sharifianjazi F, Esmaeilkhanian AH, Karimi N, Horri BA, Bazli L, Eskandarinezhad S, et al. A review of combustion properties, performance, and emission characteristics of diesel engine fueled with Al2O3 nanoparticle-containing biodiesel. Clean Techn Environ Policy 2023;26:3715–37. https://doi.org/10.1007/s10098-023-02568-2.
[23] Parveg ASMS, Ratner A. A comprehensive review of liquid fuel droplet evaporation and combustion behavior with carbon-based nanoparticles. Prog Energy Combust Sci 2025;106:101198. https://doi.org/10.1016/j.pecs.2024.101198.
[24] Youssef A, Ibrahim A. An experimental evaluation for the performance of a single cylinder CI engine fueled by a Diesel-biodiesel blend with alcohols and Zinc-Aluminate nanoparticles as additives. Mater Today Proc 2024. https://doi.org/10.1016/j.matpr.2024.04.015.
[25] Tiwari C, Dwivedi G, Verma TN. Exploring the performance and emission characteristics of a dual fuel CI engine using microalgae biodiesel and diesel blend: a machine learning approach using ANN and response surface methodology. Environ Dev Sustain 2024. https://doi.org/10.1007/s10668-024-05362-2.
[26] Le TT, Venugopal IP, Truong TH, Cao DN, Le HC, Nguyen XP. Effects of CeO2 nanoparticles on engine features, tribology behaviors, and environment. Energy Sources, Part A Recover Util Environ Eff 2023;45:8791–822. https://doi.org/10.1080/15567036.2023.2231387.
[27] Azam S, Park SS. Impact of Biosynthesized CeO2 Nanoparticle Concentration on the Tribological, Rheological, and thermal Performance of Lubricating Oil. Lubricants 2024;12. https://doi.org/10.3390/lubricants12110400.
[28] Singh AK, Pali HS, Singh NK, Kumar S, Sharma A. Evaluation of statistical and machine learning analysis on CRDI engine using ternary fuel doped with cerium oxide nanoadditives. Energy Convers Manag 2024;316:118823. https://doi.org/10.1016/j.enconman.2024.118823.
[29] Tamrat S, Ancha VR, Gopal R, Nallamothu RB, Seifu Y. Emission and performance analysis of diesel engine running with CeO2 nanoparticle additive blended into castor oil biodiesel as a substitute fuel. Sci Rep 2024;14:1–12. https://doi.org/10.1038/s41598-024-58420-0.
[30] Anjaneya G, Sunil S, Rao KS, Manjunatha NK, Giri J, Al-Lohedan HA, et al. Performance analysis and optimization of thermal barrier coated piston diesel engine fuelled with biodiesel using RSM. Case Stud Therm Eng 2024;57:104351. https://doi.org/10.1016/j.csite.2024.104351.
[31] Shaisundaram VS, Saravanakumar S, Balambica V, Sendil Kumar D, Chandrasekaran M, Muraliraja R, et al. Effects of thermal barrier coating using various dosing levels of aluminium oxide nanoadditive fuel on diesel in compressed ignition engine. J Nanomater 2022; 2022.. https://doi.org/10.1155/2022/8355098.
[32] Koutsakis G, Ghandhi JB. Optimization of thermal barrier coating performance and durability over a drive cycle. Int J Engine Res 2023;24:1446–63. https://doi.org/10.1177/14680874221089072.
[33] Khanam S, Khan O, Ahmad S, Sherwani AF, Khan ZA, Yadav AK, et al. A Taguchi-based hybrid multi-criteria decision-making approach for optimization of performance characteristics of diesel engine fuelled with blends of biodiesel-diesel and cerium oxide nano-additive. J Therm Anal Calorim 2024;149:3657–76. https://doi.org/10.1007/s10973-024-12918-x.
[34] Wu Q, Xie X, Wang Y, Roskilly T. Experimental investigations on diesel engine performance and emissions using biodiesel adding with carbon coated aluminum nanoparticles. Energy Procedia 2017;142:3603–8. https://doi.org/10.1016/j.egypro.2017.12.251.
[35] Dharsini PSP, Ahalya N, Kaliappan S, Sekar S, Patil PP, Pragna V, et al. Performance and environmental effects of CeO2/ZrO2 nanocomposite in triple blend methyl ester of pumpkin and neem seed oil dosed with diesel on IC Engine. J Nanomater 2022; 2022.. https://doi.org/10.1155/2022/5736453.
[36] Chandran M, Chinnappan R, Parthipan N, Ang CK. Effect of nano cerium oxide additive with tire oil blends on diesel engine combustion and emissions parameters with soot morphology analysis. Energy Sources, Part A Recover Util Environ Eff 2020;46:15235–47. https://doi.org/10.1080/15567036.2020.1810179.
[37] Krishnamoorthi T, Sampath S, Saravanamuthu M, Vengadesan E, Dillikannan D. Combined influence of thermal barrier coating and nanoparticle on performance and emissions of DI diesel engine fueled with neat palm oil biodiesel: an experimental, statistical and energy and exergy analysis. Process Saf Environ Prot 2024;186:274–88. https://doi.org/10.1016/j.psep.2024.03.108.

[38] Dhinesh B, Maria Ambrose Raj Y, Kalaiselvan C, KrishnaMoorthy R. A numerical and experimental assessment of a coated diesel engine powered by high-performance nano biofuel. Energy Convers Manag 2018;171:815–24. https://doi.org/10.1016/j.enconman.2018.06.039.
[39] Gangula VR, Nandhana Gopal GR, Tarigonda H. Investigation on different thermal Barrier-Coated Piston Engines using Mahua biodiesel. J Inst Eng Ser C 2021;102:131–44. https://doi.org/10.1007/s40032-020-00621-3.
[40] Kumaravel P, Bharathiraja G, Chandramohan P, Mohan S. Effect of oxygen enrichment in the emission characteristics of yttria stabilized zirconia coated diesel engine with alumina nanoparticle additives. J Environ Nanotechnol 2025;14:366–70. https://doi.org/10.13074/jent.2025.03.2441086.
[41] Palani V, Narayanan SG, Kumar ARP. Performance on multilayered nano-structured thermal barrier-coated compression ignition engine on green diesel. J Therm Anal Calorim 2025. https://doi.org/10.1007/s10973-025-14339-w.
[42] Venkatesan EP, Murugesan P, Ellappan S, Rajendran S, Aabid A, Abbas M, et al. Effect of Kariba weed biodiesel blended with n-pentane on the chosen parameters of a ceramic-coated thermal barrier direct injection diesel engine. ACS Omega 2022;7:46337–46. https://doi.org/10.1021/acsomega.2c04937.
[43] Şahin S, Torun A. Comparison of engine performance and emission values of biodiesel obtained from waste pumpkin seeds with machine learning. Agric 2024;14. https://doi.org/10.3390/agriculture14020227.
[44] Schinas P, Karavalakis G, Davaris C, Anastopoulos G, Karonis D, Zannikos F, et al. Pumpkin (*Cucurbita pepo* L.) seed oil as an alternative feedstock for the production of biodiesel in Greece. Biomass Bioenergy 2009;33:44–9. https://doi.org/10.1016/j.biombioe.2008.04.008.
[45] Wang S, Karthickeyan V, Sivakumar E, Lakshmikandan M. Experimental investigation on pumpkin seed oil methyl ester blend in diesel engine with various injection pressure, injection timing and compression ratio. Fuel 2020;264:116868. https://doi.org/10.1016/j.fuel.2019.116868.
[46] Shaisundaram VS, Chandrasekaran M, Shanmugam M, Padmanabhan S, Muraliraja R, Karikalan L. Investigation of *Momordica charantia* seed biodiesel with cerium oxide nanoparticle on CI engine. Int J Ambient Energy 2021;42:1615–9. https://doi.org/10.1080/01430750.2019.1611657.
[47] Hari Krishna K, Karthikeyan C. Thermal barrier coated piston experimental investigation in di diesel engines fueled with transformer oil and nanoparticle (alumina). Rev Mater 2024;29. https://doi.org/10.1590/1517-7076-RMAT-2024-0442.
[48] Yadav GPK, Bandhu D, Reddy KJ, Reddy RM, Srinivasu C, Katam GB. Performance evaluation of a thermal barrier-coated CI engine using waste oil biodiesel blends. Renew Energy Res Appl 2023;5:181–93. https://doi.org/10.22044/rera.2023.12828.1206.
[49] Holman JP. Experimental techniques for engineers. 8th ed. Tata McGraw-Hill; 2010.
[50] V. S. S, Sengottaiyan S, Raji G, S. K, M. C. Machine Learning-Driven Energy Efficiency Enhancement and Emission Reduction in Diesel Engines Using Pumpkin Seed Biodiesel Blends and CeO2 Nanoparticles. Int J Energy Res 2025;2025:2329925. https://doi.org/https://doi.org/10.1155/er/2329925.
[51] Vidyasagar Reddy G, Krupakaran RL, Tarigonda H, Raghurami Reddy D, Lakshmi KK. Optimization of performance and emission characteristics of 7% YSZ coated diesel engine with biodiesel using Taguchi method. Mater Today Proc 2023. https://doi.org/10.1016/j.matpr.2023.04.568.
[52] Sengottaiyan S, Subbarayan S, Natarajan R, Gurunathan V. Enhancing mechanical, degradation, and tribological properties of biocomposites via treatment and alumina content. J Reinf Plast Compos 2025:07316844251321664. https://doi.org/10.1177/07316844251321664.
[53] Vinothkannan V, Pushparaj T. Performance and emission characteristic analysis of Cucurbita Pepo L. and Tectona grandis seed oil biodiesel blends in Ci Engine with Additive. Energy Sources, Part A Recover Util Environ Eff 2020;47:2978–92. https://doi.org/10.1080/15567036.2020.1849453.